JOURNAL OF GEOPHYSICAL RESEARCH, VOL. ???, XXXX, DOI:10.1029/,

Decadal Variability of the Tropical Stratosphere: Secondary Influence of the El Niño-Southern Oscillation

L. L. Hood and B. E. Soukharev

Lunar and Planetary Laboratory, University of Arizona, Tucson, Arizona, USA

J. P. McCormack

Naval Research Laboratory, Washington, D. C., USA

L. L. Hood and B. E. Soukharev, Lunar and Planetary Laboratory, University of Arizona, 1629 E. University Blvd., Tucson, AZ 85721, USA (lon@lpl.arizona.edu; boris_soukharev@hotmail.com); J. P. McCormack, Naval Research Laboratory, Code 7646, 4555 Overlook Ave. SW, Washington, D. C., 20375, USA (mccormack@nrl.navy.mil).

Report Documentation Page

Form Approved
OMB No. 0704-0188

1. REPORT DATE	2. REPORT TYPE	3. DATES COVERED
2010		**00-00-2010 to 00-00-2010**

4. TITLE AND SUBTITLE	5a. CONTRACT NUMBER
Decadal Variability of the Tropical Stratosphere: Secondary Influence of the El Nino-Southern Oscillation	5b. GRANT NUMBER
	5c. PROGRAM ELEMENT NUMBER
6. AUTHOR(S)	5d. PROJECT NUMBER
	5e. TASK NUMBER
	5f. WORK UNIT NUMBER
7. PERFORMING ORGANIZATION NAME(S) AND ADDRESS(ES) **Naval Research Laboratory,Code 7646,4555 Overlook Ave. SW,Washington,DC,20375**	8. PERFORMING ORGANIZATION REPORT NUMBER
9. SPONSORING/MONITORING AGENCY NAME(S) AND ADDRESS(ES)	10. SPONSOR/MONITOR'S ACRONYM(S)
	11. SPONSOR/MONITOR'S REPORT NUMBER(S)

12. DISTRIBUTION/AVAILABILITY STATEMENT
Approved for public release; distribution unlimited

13. SUPPLEMENTARY NOTES
Journal Geophysical Research, in press, 2010

14. ABSTRACT
see report

15. SUBJECT TERMS

16. SECURITY CLASSIFICATION OF:			17. LIMITATION OF ABSTRACT	18. NUMBER OF PAGES	19a. NAME OF RESPONSIBLE PERSON
a. REPORT **unclassified**	b. ABSTRACT **unclassified**	c. THIS PAGE **unclassified**	**Same as Report (SAR)**	**61**	

Abstract. A decadal variation of tropical lower stratospheric ozone and temperature has previously been identified that correlates positively with the 11-year solar activity cycle. However, the El Niño-Southern Oscillation (ENSO) also influences lower stratospheric ozone / temperature. It is therefore legitimate to ask whether quasi-decadal ENSO variability can contribute to this apparent solar cycle variation, either accidentally because of the short measurement record (e.g., Marsh and Garcia [2007]) or physically because solar variability affects ENSO. Here, we present multiple regression analyses of available data records to compare differences in results obtained with and without including an ENSO term in the statistical model. In addition, simulations are performed using the NRL NOGAPS-ALPHA GCM for warm/cold ENSO conditions to test for consistency with the ENSO regression results. We find only very minor changes in annual mean solar regression coefficients when an ENSO term is included. However, the observed tropical ENSO response provides useful insights into the origin of the unexpected vertical structure of the tropical solar cycle ozone response. In particular, the ENSO ozone response is negative in the lower stratosphere due to increased upwelling but changes sign, becoming positive in the middle stratosphere ($5 - 10$ hPa) due mainly to advective decreases of temperature and NO_x, which photochemically increase ozone. A similar mechanism may explain the observed lower stratospheric solar cycle ozone / temperature response and the absence of a significant response in the tropical middle stratosphere.

1. Introduction

Continuous global satellite measurements beginning in late 1978 show a decadal variation of total column ozone at tropical and subtropical latitudes that is approximately in phase with the solar cycle (Figure 1b). Observations also indicate a significant solar cycle temperature variation in both the upper stratosphere [e.g., McCormack and Hood, 1996] and in the lower stratosphere [e.g., Steinbrecht et al., 2003; Labitzke, 2004; Crooks and Gray, 2005; Randel et al., 2009a; Gray et al., 2009]. However, the shortness of the record and the occurrence of two major volcanic eruptions following the first two solar maxima (El Chichón in early April of 1982 and Pinatubo in June of 1991) has led to questions about whether the ozone response to volcanic aerosol injections could alias or even be confused with the response to the 11-year solar cycle [Solomon et al., 1996; Lee and Smith, 2003]. This is especially true since the statistical method that has been most commonly applied to estimate empirically the solar component of stratospheric interannual variability is multiple linear regression, which makes the simplified assumption that all forcings are orthogonal, i.e., independent of one another, and that all responses are linear [e.g., Stolarski et al., 1991; Hood and McCormack, 1992; Hood et al., 1993; Reinsel et al., 2005].

These concerns have fortunately been mitigated in recent years by the absence of major eruptions since 1991 and a continuation of the decadal ozone variation for one additional cycle. Moreover, extensions of the total ozone record backward in time using ground-based Dobson spectrophotometer data have supported the existence of a decadal ozone variation for at least several more cycles prior to the start of continuous satellite data [WMO, 2007,

Chapter 3]. Consequently, the existence of a significant solar cycle variation of total ozone (and, by extension, the stratosphere as a whole) has become clearer in recent years [e.g., WMO, 2007; Gray et al., 2010].

Nevertheless, the vertical structure of the stratospheric solar cycle variation remains poorly understood. Prior to 2006, most or all published model simulations of the tropical solar cycle ozone variation were characterized by a broad response maximum centered in the middle stratosphere (5 - 10 hPa) that was caused mainly by increased photolysis of molecular oxygen by solar UV radiation (see, e.g., Hood [2004] and Chapter 3 of WMO [2007] for reviews). In contrast, the observationally estimated tropical ozone response is characterized by a double-peaked vertical structure with solar min-to-max amplitudes of several per cent in the upper and lower stratosphere but no statistically significant response in the middle stratosphere (e.g., McCormack and Hood [1996]). It was not clear whether the disagreement between models and observations was due to a model shortcoming or to problems with the observations [e.g., Lee and Smith, 2003].

To address this issue, an improved analysis of three independent satellite ozone datasets with lengths extending up to 25 years was carried out [Soukharev and Hood, 2006 (hereafter SH06); see also Randel and Wu, 2007]. Column ozone measurements were also compared with Upper Atmosphere Research Satellite (UARS) Halogen Occultation Experiment (HALOE) ozone profile data during the 1992-2003 period when no major volcanic eruptions occurred to test the conclusion that most of the solar cycle total ozone variation occurred in the lower stratosphere. Separate time intervals were analyzed using the longest (25-year) data record to test the reproducibility of the solar regression coefficients. Results confirmed that the basic vertical structure of the derived solar cycle

ozone response was the same during the last half (post-Pinatubo) part of the record as it was during the first half and that most of the solar cycle column ozone variation occurred in the lower stratosphere. Overall, therefore, the analysis supported the reality of the double-peaked ozone profile response to the solar cycle.

Consistent with the weight of the observational evidence, simulations by coupled chemistry climate models (CCM's) have begun to produce a double-peaked ozone profile response that is qualitatively similar to that which is observed [e.g., Austin et al., 2008; Matthes et al., 2007]. The main improvements in the latter simulations were: (a) Integration of each CCM forward in time ("transient simulations"); and (b) forcing the models with observed sea surface temperatures (SST's). However, the specific physical mechanisms that are responsible for this better agreement are difficult to identify from the CCM simulations alone.

Most current mechanisms for explaining a solar cycle variation in the lower stratosphere involve "downward control" from the upper atmosphere. These include (a) influences of observed 11-year variations in the lower mesospheric subtropical jet on the timing (early winter vs. late winter) of sudden stratospheric warmings, which in turn modulate the Brewer-Dobson circulation [Kodera and Kuroda, 2002; Matthes et al., 2004; 2006; Gray et al., 2006; Ito et al., 2009]; and (b) solar-induced changes in the duration of the west phase of the QBO [McCormack et al., 2007, and references therein]. However, it is also possible that "feedbacks from below" are a significant contributing cause. Recent experiments using global climate models have shown that both solar UV forcing of the stratosphere and an amplifying, coupled ocean-troposphere response (driven by indirect effects of solar UV forcing as well as direct effects of total irradiance forcing) must be included to simulate

the magnitude of observed 11-year climate signals in the tropical Pacific [Meehl et al., 2009]. The observationally estimated surface response to positive maxima in 11-year solar forcing resembles that observed during cold ENSO events although there are important differences [van Loon et al., 2007; van Loon and Meehl, 2008]. Other authors have also obtained observational evidence for a small solar cycle signal in global SST's [White and Liu, 2008, and references therein] as well as in equatorial tropospheric temperatures [Salby and Callaghan, 2006]. In contrast, there is no evidence for solar forcing of ENSO itself since solar flux and ENSO indices do not correlate significantly over long ($>$ 25-year) time periods. Nevertheless, these observational and climate model studies suggest that feedbacks from the amplifying ocean-troposphere response may be involved in producing the unexpected lower stratospheric ozone and temperature responses. This possibility may be consistent with the need to use observed SST's as a lower boundary condition in CCM simulations that successfully produce a second lower stratospheric solar ozone response maximum [e.g., Austin et al., 2008].

However, a study using the National Center for Atmospheric Research (NCAR) Whole Atmosphere Community Climate Model (WACCM) has suggested that aliasing from the El-Niño / Southern Oscillation (ENSO) could be causing part of the apparent positive solar cycle ozone response in the tropical lower stratosphere [Marsh and Garcia, 2007]. It was pointed out that, over the 1979 - 2003 time period, the Niño 3.4 ENSO index (N3.4) was almost significantly correlated (R $\simeq$ - 0.19 at a lag of -6 months) with solar UV proxies such as the 10.7 cm radio flux (F10.7). Since F10.7 and N3.4 may not therefore have been entirely orthogonal during this time period, some aliasing of the ENSO response onto the solar cycle response could have occurred. In support of this possibility, multiple

regression analyses of WACCM model output with and without including an ENSO proxy term with a suitable time lag in the regression model showed that including the ENSO term reduced considerably the apparent solar cycle ozone response at levels below 20 hPa. Since the statistical model of SH06 did not include an ENSO term, the same aliasing could potentially exist for the ozone response derived from observations.

In this paper, new multiple regression analyses are reported of available long-term satellite remote sensing data records using an improved statistical model that includes an ENSO term. In addition, time-progressive simulations using the Naval Research Laboratory (NRL) NOGAPS-ALPHA general circulation model (GCM) are carried out for warm and cold ENSO conditions to allow comparisons with the ENSO regression results. The main objectives are (a) to investigate whether aliasing from ENSO contributes significantly to the solar cycle ozone response derived from observations; and (b) to investigate more completely the response of the tropical stratosphere to ENSO forcing using both observational analyses and model simulations. We find that the ENSO response in both the lower and middle stratosphere provides useful insights into the origin of the unexpected vertical structure of the tropical solar cycle ozone response.

The paper is organized as follows. In section 2, the existence of both solar cycle and ENSO components of decadal stratospheric variability is first illustrated using representative total ozone time series. The adopted multiple regression statistical model is described and the existence of any significant aliasing of the solar cycle ozone profile response by ENSO is tested by analyzing data with and without inclusion of an ENSO term. In section 3, the statistical model is applied to estimate ENSO regression coefficients for the ozone profile, temperature, zonal wind, and total ozone using available long-term data

sets. The geographic and seasonal dependences of the total ozone ENSO coefficient are also estimated. In section 4, model calculations for strong and weak ENSO conditions are carried out using the NOGAPS-ALPHA model to allow comparisons with the observationally derived ENSO regression coefficients. In section 5, likely physical mechanisms for explaining the vertical structures of the ENSO regression results are discussed. Possible implications for the origin of the vertical structure of the solar cycle ozone response are also examined. A summary and further discussion are given in section 6.

2. Statistical Separation of the ENSO and Solar Responses

Figure 1 compares several zonal averages of the Total Ozone Mapping Spectrometer / Solar Backscattered Ultraviolet (TOMS/SBUV) total ozone record compiled and calibrated at Goddard Space Flight Center by S. Frith and R. Stolarski (http://code916.gsfc.nasa.gov/Data_services; Frith and Stolarski [2005]) with the solar Mg II UV index (ftp://ftp.ngdc.noaa.gov/STP/SOLAR_DATA/SOLAR_UV; Viereck and Puga [1999]). In Figure 1a, which plots a nearly global (65°S to 65°N) average of the data, at least three sources of decadal variability can be seen. First, there is a long-term, at least partly anthropogenic, trend. This trend was roughly linear and negative until the late 1990's but has since been noticeably reduced in amplitude [WMO, 2007, Chapter 3]. Second, significant ozone decreases occur following the major volcanic eruptions of El Chichón in late March / early April of 1982 and Pinatubo in June of 1991 [Solomon et al., 1996; Robock, 2000; Stenchikov et al., 2002]. Third, there is a tendency for higher global ozone averages near maxima of the 11-year solar cycle [Hood and McCormack, 1992; Hood, 1997; Zerefos et al., 1997; Soukharev and Hood, 2006; Randel and Wu, 2007; Tourpali et

al., 2007]. The volcanic and trend contributions are strongest at middle and high latitudes where heterogeneous chemical losses and dynamical transport are most important (e.g., Brasseur and Solomon [2005]). However, at low latitudes, the solar contribution appears to dominate. This is illustrated in Figure 1b, which plots a tropical and subtropical (35°S to 35°N) average time series.

The El-Niño / Southern Oscillation is an oscillation of the coupled atmosphere and ocean system (primarily in the tropical Pacific) that is arguably the dominant global mode of interannual climate variability [e.g., Brönnimann, 2007]. Warmer SST's during an El-Niño event produce increased convection, increased latent heat release, a warmer troposphere, and a higher tropopause particularly over the eastern tropical Pacific but also throughout the tropics. The opposite is the case for La Niña. Evidence for an ENSO contribution to total ozone variability in the tropics was first obtained using Nimbus 4 BUV data [Hasebe, 1983] and the geographic dependence of the variation was first estimated using Nimbus 7 TOMS data [Shiotani, 1992; Randel and Cobb, 1994].

Figure 2 compares a tropical zonal average (20°S to 20°N) of the Version 8 TOMS/SBUV record with the Niño 3.4 index (sea surface temperature anomaly averaged over the 5°S to 5°N and 120°W to 170°W sector). A number of distinct positive (El-Niño) and negative (La Niña) events can be seen in Figure 2b. Note that El-Niño peaks tend to occur in early boreal winter. The peaks in the N3.4 index in Figure 2b are often accompanied by decreases several months later in ozone in Figure 2a. For example, a sharp tropical ozone decrease occurs several months following the El-Niño event of late 1997. This ozone reduction is generally understood to be caused by increased tropical upwelling following warm events (see section 5.1 below). However, dynamically induced interannual

ozone variability from other sources (notably from the equatorial quasi-biennial wind oscillation, or QBO) is large in the tropics. Consequently, the best correlation between tropical TOMS/SBUV zonal mean column ozone and the Niño 3.4 ENSO index is only $R = -0.37$ (significant at 99% confidence) at 4 months positive lag (ozone lags ENSO). In general, Figures 1 and 2 suggest that ENSO is secondary in importance to solar and volcanic forcing for driving decadal variability of the tropical stratosphere.

2.1. Regression Model

In order to represent the temporal behavior of a given stratospheric variable, $X(t)$, we consider a multiple linear regression model with a form similar to that used in previous work (SH06 and references therein), but with the addition of an ENSO term and including a more complete representation of the QBO:

$$X(t) = \mu(i) + \beta_{trend}t + \beta_{QBO1}u_{30hPa}(t - lag_{QBO1}) + \beta_{QBO2}u_{10hPa}(t - lag_{QBO2})$$

$$+\beta_{volcanic}Aerosol(t) + \beta_{solar}MgII(t) + \beta_{ENSO}N3.4(t - lag_{ENSO}) + \epsilon(t) \qquad (1)$$

where t is the time in months (for ERA-40 and TOMS/SBUV) or 3-month seasonal increments (for ozone profile datasets), $\mu(i)$ is the long-term mean for the ith month ($i = 1, 2, ...12$) or season ($i = 1, 2, ...4$) of the year; u_{30hPa} and u_{10hPa} are the 30 and 10 hPa equatorial zonal winds obtained from National Centers for Environmental Prediction (NCEP) reanalysis data [Kalnay et al., 1996]; lag_{QBO1} and lag_{QBO2} are lag times required to produce a maximum positive or negative correlation between the $X(t)$ time series at a given location and the 30 and 10 hPa equatorial winds; $Aerosol(t)$ is a stratospheric aerosol index based on a combination of SAM II and Stratospheric Aerosol and Gas Experiment (SAGE) I/II optical depth measurements [Thomason et

al., 1997]; $MgII(t)$ is the core-to-wing ratio of the solar Mg II line at 280 nm based on Nimbus 7 SBUV, NOAA 9 and 11 SBUV/2, and UARS SUSIM data [e.g., Viereck and Puga, 1999]; N3.4 is the Niño 3.4 index (defined as above and available from: http://www.cgd.ucar.edu/cas/catalog/climind/Nino_3_3.4_indices.html); lag_{ENSO} is a lag time required to produce a maximum correlation amplitude between $X(t)$ and N3.4; and $\epsilon(t)$ is a residual error term. The coefficients β_{trend}, β_{QBO1}, β_{QBO2}, $\beta_{volcanic}$, β_{solar}, and β_{ENSO} are determined by least squares regression. The aerosol index term is included in the model only for levels at 10 hPa and below.

As in previous work, to avoid overestimation of regression coefficients and their statistical significance, it is important to model the residual error term as an autoregressive process, e.g., for a first-order process, $\epsilon(t) = r\epsilon(t-1) + w(t)$, where $w(t)$ is white noise and r is determined in an initial application of (1) (e.g., Neter et al. [1985]). Crooks and Gray [2005] have modeled the error term as a third-order autoregressive process to be more complete; however, they find no difference in the results if other orders are used instead. A first-order process is therefore considered to be sufficient here.

There are several alternate methods for representing the QBO in multiple regression statistical models. A single QBO term proportional to the 30 hPa equatorial wind and with an optimum phase lag has been found to be adequate for evaluating the solar cycle ozone variation [SH06]. However, for the purpose of evaluating solar cycle or ENSO zonal wind and temperature variations, a more complete QBO representation is necessary. In particular, it is preferable to include two separate QBO terms that account for the out-of-phase relationship between QBO winds in the upper and lower stratosphere (e.g., Randel and Wu [1996]; Crooks and Gray [2005]; Shibata and Deushi [2008]). Randel and Wu

[2007; 1996] have used the first two QBO empirical orthogonal functions (EOF's) derived from equatorial zonal wind data at all levels to represent the QBO in their regression model. On the other hand, Shibata and Deushi [2008] and Steinbrecht et al. [2003] have used the actual QBO equatorial winds at two different levels to represent the QBO. The former authors used 50 and 20 hPa winds while the latter authors used 30 and 10 hPa winds. The winds at either of these two levels are about one quarter cycle out of phase indicating that they can be treated as approximately independent variables. In the present work, we follow Steinbrecht et al. and use actual QBO equatorial winds at the 30 and 10 hPa levels but with small lag times added to further maximize the projection of $X(t)$ onto the QBO. Several experimental analyses were carried out using either the orthogonal time series of Randel and Wu (private communication, 2008) or the actual winds at various levels (50 and 20 hPa, 30 and 10 hPa). It was found that there is no statistically significant difference in the results for the solar and ENSO zonal wind and temperature regression coefficients when any of these three methods is applied.

2.2. Tests for ENSO Aliasing

The zonal mean ozone profile response to the 11-year solar activity cycle has previously been estimated by a number of analysts using mainly satellite remote sensing data (e.g., Hood et al. [1993]; Chandra and McPeters [1994]; McCormack and Hood [1996]; Wang et al. [1996]; Soukharev and Hood [2006]; Randel and Wu [2007]; Tourpali et al. [2007]). However, as mentioned in the Introduction, it has been found using WACCM model output that the solar cycle ozone regression coefficient in the lower stratosphere decreases significantly when an ENSO term is included in the statistical model, suggesting aliasing between the ENSO and solar cycle terms. To test whether this also occurs in actual

stratospheric data, we have re-calculated the annual mean solar regression coefficient using the same data sets analyzed previously by SH06.

Figure 3 shows results of an application of (1) with and without inclusion of the ENSO term to the 3-month SBUV(/2) zonal mean ozone profile time series over the 1979 to 2003 period (see SH06 for a description of this data set). The annual mean regression coefficient obtained without the ENSO term (top panel) is compared to that obtained with the ENSO term at an optimum lag of +3 months (bottom panel). They are nearly identical and there is no significant change in the coefficients in the lower stratosphere. The vertical structure in the tropics, consisting of positive responses in the upper and lower stratosphere but no significant response in the middle stratosphere, differs from that expected from photochemical effects alone [SH06]; possible explanations for this difference are discussed in section 5.3. Similar applications to other stratospheric data (SAGE II and HALOE ozone profile data, ECMWF ERA-40 temperatures and winds) also yield only slightly altered annual mean solar regression coefficients with and without inclusion of an ENSO term (not shown here). Figure 4 directly compares the tropically averaged solar cycle ozone regression coefficients calculated from the three ozone satellite data sets (SBUV, UARS HALOE, and SAGE II) using (1) with and without an ENSO term at optimum lag (3 months since the time series are seasonal rather than monthly). The changes that result from addition of the ENSO term are all much less than the 2σ error bars. Comparisons of the SBUV(/2) results with those of SAGE II and HALOE are necessary since SBUV does not adequately resolve the ozone profile in the lowermost stratosphere [Bhartia et al., 1996; SH06].

We have also investigated whether any significant aliasing between the ENSO and solar cycle terms could occur when only data for individual seasons are analyzed. For three of the four seasons, solar cycle ozone regression coefficients obtained with and without an ENSO term are nearly identical, as is the case in Figures 3 and 4. However, for northern winter data, some significant differences are found (Figure 5). Specifically, the DJF responses in the lower stratosphere where (1) is applied with an ENSO term (Figure 5b) are weakened between $\sim$ 20°S and 30°N by as much as 25% and the regions of statistical significance are smaller. Also, in the upper stratosphere, the maximum solar cycle ozone response increases from $\sim$ 4% to $\sim$ 5%. As mentioned above in relation to Figure 2, ENSO events tend to peak during boreal winter and have especially large effects in the eastern Pacific region. It is therefore not unexpected that aliasing from ENSO would preferentially occur during this season and/or at certain longitudes where ENSO forcing is more prominent.

As a further test, column ozone solar regression coefficients were calculated as a function of longitude, latitude, and season using the version 8 TOMS/SBUV data set. Again, for the boreal spring, summer, and fall seasons, only very minor differences were noted when an ENSO term was added to the regression model. However, during boreal winter (DJF), more significant differences were noted. As seen in Figure 6, the resulting regression coefficients are slightly altered and the total region where the coefficients are significant (shaded area) is somewhat larger when the ENSO term is included. However, the general character and distribution of the DJF solar regression coefficient are approximately the same in Figures 6a and 6b.

On this basis, it is concluded that aliasing from ENSO produces only minor changes in annual mean solar cycle regression coefficients calculated from available stratospheric data during the 1979-2003 period. The annual mean and most of the seasonal ozone profile solar regression coefficients obtained previously (e.g., SH06) are therefore still approximately valid. Only during boreal winter (DJF) are significant evidences obtained for limited ($<$ 25%) aliasing of solar regression coefficients at certain latitudes, longitudes, and pressure levels. The overall lack of sensitivity of the observational solar cycle regression coefficients to whether an ENSO term is included in the statistical model is partly because of other sources of interannual variability (e.g., the QBO) in actual stratospheric time series, which obscure the ENSO influence. Another contributing factor is probably that the WACCM model overestimates somewhat the actual ozone sensitivity to ENSO in parts of the lower stratosphere (see next section).

3. ENSO Regression Coefficients

Figure 7 plots the annual mean Version 8 SBUV(/2) ozone profile ENSO regression coefficient for the 1979-2003 period, expressed in per cent change of ozone for a 1 unit (i.e., 1° C) positive change of the N3.4 index. The plot was produced by applying (1) successively to the 3-month average SBUV(/2) data at individual latitude/pressure grid points. It was found empirically that a maximum correlation between the N3.4 index and the ozone time series is obtained at a majority of grid points for a positive phase lag (L_{ENSO}) of 1 time unit (3 months). The responses shown are therefore at a phase lag of 3 months (ozone lags ENSO). Shaded areas indicate grid points where the ENSO regression coefficient is significant at the 95% confidence level. As seen in Figure 2, a 1 unit increase

in N3.4 corresponds to a modest warm (El-Niño) event in the eastern tropical Pacific while a 2 to 2.5 unit increase corresponds to a strong El-Niño event. Therefore, to estimate the true ozone response to a strong El-Niño event, the values in the tropical lower and middle stratosphere shown in Figure 7 should be multiplied by a factor of 2 or 2.5. Figure 8 plots the corresponding regression coefficients obtained using SAGE II data over the 1985-2003 period and UARS HALOE data over the 1992-2003 period. For the SAGE II analysis, the period immediately following the Pinatubo eruption (from JJA 1991 to SON 1993) is excluded from consideration in lieu of including an aerosol term in the regression model [SH06].

In Figure 7, a large region of significant negative SBUV(/2) response is obtained in the tropical lower stratosphere while a zone of positive response is obtained in the equatorial middle stratosphere. Similar patterns are seen in Figures 8a and 8b, although less distinct, apparently due to the reduced record lengths and/or sampling of the SAGE II and HALOE data. In all three plots, but especially in the SAGE II and HALOE plots, the zone of positive response tends to be shifted noticeably toward the Northern Hemisphere. As will be discussed in section 5, both the negative ozone response in the lower stratosphere and the positive response in the equatorial middle stratosphere are consistent with a net positive increase in tropical upwelling rate following El-Niño events. In addition, a zone of apparently significant positive response is obtained at low latitudes above the stratopause in Figure 7. However, no corresponding response is seen in the SAGE II and HALOE plots of Figure 8.

Table 1 lists the tropical mean (24°S to 24°N) ENSO ozone regression coefficients at five lower stratospheric levels as calculated here by applying (1) to the SBUV/2, SAGE

II, and HALOE ozone profile data sets (Figures 7 and 8). Also listed is the mean ozone concentration (in Dobson Units, DU, per km) at each level as well as the ENSO ozone coefficients calculated by Marsh and Garcia for the 1979-2003 period (see their Figure 4). Although direct comparisons are not straightforward (due to the different regression models that were employed), at several pressure levels the WACCM coefficients appear to be somewhat larger than those estimated here from satellite data records. Note that the largest percentage responses are found in the lowermost stratosphere ($\sim$ 70 hPa) but the ozone concentration at this level is relatively low.

Randel et al. [2009b] have also recently estimated SAGE II ENSO ozone regression coefficients in the tropical stratosphere and have compared these coefficients to those calculated from WACCM model data. They employed a Multivariate ENSO Index (MEI) rather than N3.4 and the SAGE II record analyzed was slightly longer than that considered here. (Note that the mean MEI value for El-Niño events in a given period is lower than the mean N3.4 value in the same period.) Just above the equatorial tropopause ($\sim$ 80 hPa; $\sim$ 17.7 km), a large percentage response maximum was obtained with a peak amplitude of > 7 %/MEI using either SAGE data or WACCM data (compare with Figure 8a). However, the ozone concentration at this level ($\sim$ 2.3 DU/km) is lower than at higher altitudes in the lower stratosphere (peaking at nearly 18 DU/km near 20 hPa; see Table 1). Similar coherent patterns were also found in both the SAGE II and WACCM coefficients at middle latitudes but these coherent patterns were at altitudes below $\sim$ 15 km where the mean ozone concentration is again low. Above 20 km altitude where the tropical ozone concentration is large, a careful reading of their Figure 4 shows that the ENSO ozone coefficients estimated from WACCM model data are somewhat larger than those

calculated from SAGE II data. For example, at 50 hPa, the equatorial SAGE II ENSO coefficient is $\sim$ 2 %/MEI while that estimated from WACCM data is $\sim$ 3.4 %/MEI. At 40 hPa, the equatorial SAGE II value is $\sim$ 1.1%/MEI while the corresponding WACCM value is nearly 2%/MEI. At 30 hPa where the tropical ozone concentration approaches 16 DU/km, the equatorial SAGE II value is less than 1%/MEI while the corresponding WACCM value is $\sim$ 2%/MEI. Therefore, at levels in the lower stratosphere where the ozone concentration is large, their results appear to be qualitatively similar to those shown in Table 1.

In order to estimate the response of zonal mean stratospheric temperature and zonal wind to ENSO, we consider the ECMWF ERA-40 temperature and derived zonal wind data set extending from 1979 through 2001. Annual mean results from the multiple linear regression analysis are shown in Figure 9. Latitudes from 60°S to 60°N are given to be consistent with the ozone response results of Figures 7 and 8. Regression coefficients are shown at pressures from 100 to 1 hPa, which differ slightly from those for the ozone response plots (50 to 0.5 hPa). In the tropics, the ENSO temperature plot (Figure 9a) is characterized by a negative response in the lowermost stratosphere (centered in the 50 to 70 hPa range). This negative response is similar to the lower stratospheric ENSO temperature response estimate derived originally from radiosonde data by Reid et al. [1989] and Reid [1994] (see also Free et al. [2009] and Randel et al. [2009b]). However, the amplitude of the radiosonde-derived temperature response in the western tropical Pacific was of the order of -1 K for a change of one standard deviation of the El-Niño SST index in the 40 to 80 hPa range (comparable to a change in N3.4 of 1 unit) [Reid, 1994]. In contrast, the zonally averaged amplitude derived from the ERA-40 data is only

about −0.1 K for an increase in N3.4 of 1 unit. The zonal wind response to positive ENSO forcing (Figure 9b) is characterized by enhancements of the subtropical upper tropospheric jets.

The annual mean TOMS/SBUV total ozone ENSO regression coefficient is plotted in Figure 10. The largest region of statistically significant response has a negative amplitude and is located in the tropical eastern Pacific ($\sim$ 30°S to 30°N; $\sim$ 80°W to 180°W). Note the two negative anomaly maxima centered on the equator in the tropics. This pattern resembles that obtained from analyses of Microwave Sounding Unit temperature data [Yulaeva and Wallace, 1994; Calvo-Fernandez et al., 2004]; the latter authors interpret this structure as a wave pattern that mirrors the structure in the troposphere. Positive responses with amplitudes comparable to those of the tropical negative responses are obtained at middle latitudes in the same longitude sector. As discussed further in section 5, this latitude dependence implies ENSO-related influences on the residual meridional circulation (see also Free et al. [2009], and section 5.1). The seasonal dependence of the total ozone ENSO coefficients is shown in Figure 11. It is evident from these plots that the negative tropical eastern Pacific response is most pronounced in boreal winter (DJF) and is least pronounced in summer (JJA). The midlatitude positive responses occur mainly during boreal winter and spring. In particular, during boreal winter, the strongest positive maxima in the Northern Hemisphere (up to 2% per unit of N3.4) occur in the northern Pacific region south of Alaska. These northern Pacific response patterns may reflect ENSO influences on regional stratospheric circulation such as the strength of the Aleutian stratospheric anti-cyclone in addition to influences on the residual circulation.

4. Model Simulations for Warm/Cold ENSO Conditions

Before discussing physical mechanisms in section 5, it is useful to compare the annual mean ENSO ozone and temperature regression coefficients (Figures 7, 8, and 9a) with representative model simulations for strong/weak ENSO conditions. For this purpose, we use the Navy's Operational Global Atmospheric Prediction System (NOGAPS), which combines a global spectral forecast model with a 3D variational data assimilation system. The present study uses a high-altitude version of NOGAPS, NOGAPS-ALPHA (Advanced Level Physics-High Altitude), with parameterized chemistry [McCormack et al., 2006; Hoppel et al., 2008; Eckermann et al., 2008].

The version of NOGAPS-ALPHA used here has 68 (L68) hybrid $\sigma - p$ vertical levels extending from the surface to $5{\times}10^{-4}$ hPa ($\sim$ 100 km) with $\sim$ 2 km spacing throughout most of the stratosphere [Eckermann, 2009]. It has an effective Gaussian horizontal grid spacing of 1.5° in latitude/longitude (triangular spectral truncation up to wave number 79). Shortwave heating and longwave cooling rates due to O_3, CO_2, and H_2O from the surface to the lower mesosphere are computed using the method of Chou et al. [2001] and Chou and Suarez, 2002]. Above 90 km, non-local thermodynamic equilibrium (LTE) cooling rates due to CO_2 are calculated [Fomichev et al., 1998]. Both O_3 and H_2O are prognostic variables in the forecast model. Production and loss of O_3 and H_2O are determined using a linearized photochemistry parameterization [McCormack et al., 2006; 2008]. The model is therefore not a fully coupled CCM. In particular, while photochemical effects of temperature changes are approximately accounted for, advection of long-lived trace species such as NO_x, which significantly influence ozone concentrations in the middle and upper stratosphere, is not accounted for in the model.

The model's T79 spectral truncation cannot explicitly resolve small-scale gravity wave breaking in the middle atmosphere, which exerts a drag force on the background zonal winds and drives the circulation away from a thermal equilibrium state. Therefore, the model uses the parameterizations of Webster et al. [2003] and Garcia et al. [2007] to describe the effects of sub-grid scale orographic and non-orographic gravity wave drag, respectively. The current model has no QBO, either forced or internally generated.

The NOGAPS-ALPHA forecast model uses observed or climatological distributions of sea surface temperature and sea ice concentrations as lower boundary conditions. To determine the response of NOGAPS-ALPHA to ENSO forcing, we conducted twelve 120-day free-running model simulations with identical initial conditions. The first ensemble of six simulations used operational NOGAPS SST and sea ice values updated every 12 hours for the period 2 December 2002 – 31 March 2003 (denoted "DJF03") for the lower boundary condition. During this period, SST's in the eastern tropical Pacific were much warmer than normal (N3.4 $\simeq$ 1.22), characteristic of El-Niño conditions (see Figure 12). The second ensemble of six simulations used NOGAPS SST and sea ice for the period 2 December 2007 – 31 March 2008 ("DJF08"), when the SST's were cooler than normal (N3.4 $\simeq$ -1.72), characteristic of La Niña. Initial conditions for these simulations were generated from a 4-year model integration using monthly mean climatological SST and ice fields for boundary conditions to allow the model to reach a balanced state. Model output was saved every 12 hours throughout the simulations.

Figures 13a,b,c respectively plot the zonal mean ozone mixing ratio (ppmv), temperature (Kelvin), and vertical velocity (mm/s) differences (DJF03 − DJF08) as a function of time between the two ensemble means, averaged over the 10°S to 10°N latitude range.

Figure 14 replots the zonal mean ozone mixing ratio differences in units of per cent to allow more direct comparisons to the observational results of Figures 7 and 8 as well as to the SAGE II results of Randel et al. [2009b]. Since the difference in N3.4 between the two time periods is $\simeq 3$, all values should be divided by 3 to estimate the model response to a unit change in N3.4. In the last column of Table 1, we list the ozone differences during the final 60 days of the integrations averaged over 24°S to 24°N and expressed in units of %/N3.4.

In the case of the ozone difference plots (Figures 13a and 14), toward the end of the simulations, ozone mixing ratio differences in the stratosphere below the 15 hPa level are generally negative and range from ~ -0.13 ppmv ($\sim 2\%$) near 20 hPa to ~ -0.06 ppmv ($\sim 5\%$) near 50 hPa, i.e., the mixing ratios are reduced under El-Niño conditions. These differences are significant at >95% confidence as verified by a Student's t-test. The corresponding reductions for a 1-unit decrease in N3.4 range from ~ 0.04 to 0.02 ppmv. As shown in Table 1, the mean per cent differences per unit of N3.4 during the last 60 days of the model integrations averaged over 24°S to 24°N range from ~ -0.5 %/N3.4 at 20 hPa to ~ -1.2 %/N3.4 at 50 hPa. These model sensitivities are comparable in magnitude to the observational (e.g., SAGE II) ENSO ozone regression coefficients and are significantly less than the WACCM ENSO coefficients at most levels in the lower stratosphere where the mean ozone concentration is large.

At and above the 10 hPa level, mixing ratio differences are generally positive; mean differences in the 5 - 10 hPa pressure range are $\sim +0.15$ ppmv (~ 0.05 ppmv for a 1 unit change in N3.4), implying ozone increases under El-Niño conditions. These maximum differences are again significant at $> 95\%$ confidence. The model response vertical structure

at near-equatorial latitudes is similar to that of the observational ENSO ozone regression coefficients shown in Figures 7 and 8. For typical climatological mixing ratios at 5 - 10 hPa of $\sim$ 9 ppmv, the ozone increase derived from SBUV/2 data is about 0.5% or $\sim$ 0.05 ppmv, not much less than the mean amplitudes seen in Figures 13a and 14 after dividing by 3.

In the case of the temperature difference plot (Figure 13b), model equatorial temperature differences during the last half of the simulations are consistently largest in the 50 - 70 hPa pressure range and average about -2.5 K ($\sim$ 0.8 K per unit of N3.4). These differences are significant at $>$ 99% confidence according to a Student's t-test. As seen in Figure 9a, the observationally derived equatorial temperature difference is also largest in the 50 - 70 hPa range but the amplitude is only -0.1 K per unit of N3.4. The model differences also show lesser decreases of as much as 1.5 K ($\sim$ 0.5 K per unit of N3.4) throughout the middle and upper stratosphere, which are not seen in the regression results. On the other hand, as also noted in section 3, Reid [1994] reported temperature decreases in the western Pacific lower stratosphere of the order of -1 K for increases of one standard deviation of an SST index that may be comparable to N3.4. Also, Randel et al. [2009b] report peak equatorial temperature decreases of order -0.5 K/MEI in the same pressure range using an updated and adjusted radiosonde data set.

In the case of the vertical velocity difference plot (Figure 13c), toward the end of the simulations, model vertical velocity differences are generally positive throughout most of the stratosphere and are also positive in the upper troposphere, implying net tropical upwelling during warm events relative to cold events. Most of these velocity differences are significant at $>$ 95% confidence according to the Student's t-test. It is unlikely that

the lack of significant positive velocities in the lowermost stratosphere ($\sim$ 60 to 100 hPa) is related in any way to the model formulation. The model employs a single hybrid vertical coordinate that is terrain following very close to the surface and isobaric in the upper levels [Eckermann, 2009]. Its use reduces stratospheric errors in divergence fields compared to other coordinate systems, and so is well suited for simulating lower stratospheric vertical velocity anomalies related to higher SST's.

It should be emphasized that the absence of a QBO in the model undoubtedly simplifies the model response compared to that derived from observations. In addition, the SST's drive the model through a parameterization of cumulus convection, which is not straightforward to implement in such a model. Nevertheless, despite these caveats, the approximate agreement of the NOGAPS-ALPHA ENSO ozone sensitivities with observations (Table 1) and the similar altitude dependences of the modeled and observed ENSO ozone and temperature anomalies (Figures 7, 8, and 9a) is encouraging.

5. Physical Interpretation of the ENSO Regression Results

5.1. The Lower Stratospheric Response

As seen in the ERA-40 analysis of Figure 9a and in the NOGAPS-ALPHA temperature differences in Figure 13b, the strongest thermal response to ENSO forcing in the tropical stratosphere consists of a pronounced cooling during warm events centered near 50 - 70 hPa. Reid et al. [1989] and Reid [1994] first reported evidence for this cooling response using radiosonde data. They found that ENSO-related cooling effectively amplified the annual temperature cycle in this region, deepening the temperature minimum of the cycle, which occurs in boreal winter, while leaving the maximum nearly the same. Possible

mechanisms discussed at that time for producing the cooling response included: (a) the radiative effect of optically thick cirrus clouds associated with enhanced convective activity during warm events [Webster and Stephens, 1980]; and (b) variations in the intensity of the tropospheric Hadley circulation associated with increased SST's [e.g., Bjerknes, 1966], which could produce adiabatic temperature decreases in the lowermost stratosphere.

As shown in Figure 13c, while increased upwelling occurs in both the upper troposphere and in the lower stratosphere (50 hPa and above), vertical velocity anomalies tend to be quite weak near 60 hPa where the cooling maximizes in both the model simulations (Figure 13b) and in the observations (Figure 9a). On this basis, we suggest that the strong warm event cooling seen in the tropical lowermost stratosphere is probably mostly radiative in origin, deriving from decreases in upwelling infrared radiation reaching the lower stratosphere associated with increased clouds and higher cloud tops during El-Niño events. As noted by Reid [1994], such an explanation is thermodynamically reasonable since the tropospheric heating during warm events must be compensated by a cooling at higher altitudes if the effects of ENSO vanish above some level.

On the other hand, the negative ozone ENSO coefficients in the lower stratosphere (Figures 7 and 8) and the mildly reduced temperatures above $\sim$ 50 hPa seen in the model simulations of Figure 13b appear to be mainly caused by increased upwelling in the tropical stratosphere (Figure 13c). Free et al. [2009] have recently found evidence that the tropical lower stratospheric cooling in boreal winter during warm events is accompanied by a strong late winter warming at high latitudes. The high-latitude signal has characteristics similar to those of sudden stratospheric warmings, which are accompanied by accelerations of the Brewer-Dobson circulation. Consistently, as discussed in section 3,

column ozone ENSO regression coefficients are negative at low latitudes and positive at high latitudes in the eastern Pacific region (Figure 10). Since the Brewer-Dobson circulation is driven primarily by planetary wave activity, it can be inferred that the enhanced tropical upwelling is a result of enhanced Rossby wave activity associated with the ENSO-induced tropospheric circulation changes. In support of this explanation, several recent modeling studies have shown that increased SST's can modify quasi-stationary planetary waves in the tropics with effects on the residual circulation [e.g., Deckert and Dameris, 2008]. In particular, Garcia-Herrera et al. [2006] have studied the propagation of tropospheric ENSO-related planetary wave disturbances into the winter stratosphere using both general circulation models and the ERA-40 data. In general, warm ENSO events tend to maximize in boreal winter and produce zonally asymmetric tropospheric temperature anomalies in the tropics that propagate in the troposphere to the extratropics. The resulting midlatitude temperature anomalies then propagate vertically as planetary Rossby waves into the midlatitude stratosphere where they decelerate the westerly flow, inducing an acceleration of the residual circulation. The net consequence for the tropical stratosphere is increased upwelling rates. This mechanism is currently being examined further using the NOGAPS-ALPHA simulations described here.

5.2. The Middle Stratospheric Response

It remains to consider the origin of the positive tropical ENSO ozone response in the middle stratosphere (5 to 10 hPa) seen in the regression results of Figures 7 and 8 and in the model results of Figure 13a. A similar positive ENSO ozone response centered near 10 hPa was obtained in the analysis of WACCM model data by Marsh and Garcia [2007] who attributed it to the photochemical effects of adiabatic temperature changes

associated with increased tropical upwelling after warm events. As was emphasized in the model description of section 4, the NOGAPS-ALPHA model currently has only a parameterized chemistry scheme and therefore accounts only for ozone changes resulting from dynamical transport effects on temperature, which in turn affect reaction rates that determine the ozone photochemical balance. The positive ozone changes seen in Figure 13a above 10 hPa are therefore caused primarily by adiabatic temperature decreases (Figure 13b) associated with the upwelling rate increases during warm events (Figure 13c).

However, in the stratosphere (and in full CCM's such as WACCM), changes in upwelling rates near 10 hPa produce transport-induced changes in other trace gases with longer lifetimes than ozone. In particular, transport-induced changes in odd nitrogen occur, which can strongly influence the ozone photochemical balance by modifying catalytic loss rates. To illustrate this, Figure 15 compares zonal averages of NO_x and O_3 between 5°S and 5°N at 10 hPa as calculated from UARS HALOE sunset data over a 12-year period. A clear NO_x QBO is evident that is approximately out of phase with (and significantly correlated with) the ozone QBO (R = -0.94) [Randel and Wu, 1996; Baldwin et al., 2001]. It is therefore likely that increased tropical upwelling following warm ENSO events would lead to reduced NO_x concentrations and increased ozone in the middle stratosphere. This mechanism may even dominate over the photochemical effects of adiabatic temperature changes, as is apparently true for the QBO [Chipperfield et al., 1994].

5.3. Implications for the Solar Cycle Response

It has previously been inferred from observations that increased tropical upwelling occurs near or approaching solar minima [Kodera and Kuroda, 2002; Hood and Soukharev, 2003]. In the tropical lower stratosphere, such increased upwelling would reduce ozone

mixing ratios near solar minima, consistent with the observed second lower stratospheric ozone response maximum (e.g., Figure 3). In the tropical middle stratosphere, based on the interpretations given in the previous subsection, it is possible that the absence of a detectable solar cycle ozone response is also due to increased upwelling near solar minima, which would advectively decrease both the temperature and the odd nitrogen abundance, leading to photochemical ozone increases. Such an ozone increase near solar minima would tend to cancel the ozone decrease at that time caused by reduced photolysis of molecular oxygen by solar UV radiation. The net result would be an insignificant ozone response in the tropical middle stratosphere.

To examine this hypothesis further, it is useful to consider again the odd nitrogen and ozone time series shown in Figure 15 at the location of the ozone response minimum ($\sim$ 10 hPa, equator). According to these data, the interannual variability of both equatorial odd nitrogen and ozone at this location is dominated by an irregular QBO, making detection of the solar cycle component of variability more difficult. Model calculations (see, e.g., Figure 14 of SH06) indicate that the photochemical ozone increase from solar minimum to maximum at this level is only $\sim 2\%$. In contrast, the peak-to-peak ozone QBO amplitude seen in Figure 15b is in the range of 10 to 15%. Regressing the NO_x time series of Figure 15a against the ozone time series of Figure 15b yields $\Delta NO_x \simeq -2.9\Delta O_3$. Consequently, a transport-induced increase in NO_x of $\sim 5.8\%$ from solar minimum to maximum may be sufficient to cancel a direct solar UV-induced ozone increase of 2% at that location. Such an NO_x increase is much less than the peak-to-peak QBO-induced amplitude ($> 40\%$) seen in Figure 15a and is therefore difficult to rule out. For example, simple averaging

of the data of Figure 15a for various time periods representative of solar minimum and maximum conditions yields NO_x increases in the range of 1 to 5%.

6. Summary and Discussion

The analysis of NCAR WACCM model data for the 1979-2003 time period by Marsh and Garcia [2007] was valuable for drawing attention to possible aliasing of solar ozone regression coefficients by ENSO. In particular, they found that inclusion of an ENSO term in a regression model can produce large ($\sim$ 35%) reductions in WACCM annual mean lower stratospheric ozone solar regression coefficients (see their Figure 4). However, the present results indicate that when observed ozone records (SBUV/2, SAGE II, HALOE) are analyzed using a similar statistical model, only minor changes to annual mean coefficients (Figures 3 and 4) are obtained when an ENSO term is included. The same is true when seasonal data are analyzed for three of the four seasons. Only when data are analyzed for boreal winter (DJF), when ENSO events tend to peak, is evidence obtained for limited ($< 25\%$) ENSO aliasing of solar regression coefficients within several latitude, longitude, and pressure ranges (Figures 5 and 6).

As noted in section 2.2, a partial explanation for the stronger influence of ENSO on solar regression coefficients derived from WACCM model data is the presence in observational records of other sources of interannual variability, e.g., an irregular QBO, which would tend to obscure the ENSO signal. In addition, as discussed in section 3, it is likely that the ENSO signal in WACCM is somewhat stronger than is seen in observations at a number of levels in the lower stratosphere where the ozone concentration is high (see Table 1 and Figure 4 of Randel et al. [2009b]). Although the latter authors have shown that similar coherent positive and negative patterns of per cent ozone ENSO response are seen in both

WACCM and in SAGE II data, most of the coherent patterns occur at altitudes of 18 km and below where the ozone concentration is low. Consistent with these inferences, WACCM model ozone time series near 50 hPa (Figure 2 of Marsh and Garcia) correlate strongly with N3.4 (R = −0.7 at 4 months lag) while the ENSO signal in observed ozone records in the tropics is weaker (e.g., R = −0.37 at 4 months lag for the column ozone time series in Figure 2).

These results do not imply that the estimated solar and ENSO regression coefficients are highly accurate. The accuracy of the solar coefficients, in particular, depends also on the length of the time series, which for current satellite datasets, is limited to no more than 2 or 3 solar cycles. A completely accurate determination of the linear response may require as many as 10 cycles of high-quality global measurements. Further, it is well known that the QBO, ENSO, and solar cycle responses interact and their effects are not linear, especially at high latitudes [e.g., Garfinkel and Hartmann, 2007; Calvo et al., 2009; Labitze, 2004], which is inconsistent with the assumptions of the multiple linear regression method. Hence, even with an infinitely long time series, the solar and ENSO regression coefficients may not attain complete accuracy.

As found in section 3, the ENSO ozone regression coefficient derived from SBUV/2, SAGE II, HALOE, and TOMS data is characterized by a negative response in the tropical lower stratosphere, mainly in the eastern Pacific region over a wide range of altitudes (Figures 7, 8, and 10). The temperature coefficient is characterized by a negative response in the lower stratosphere that is statistically significant within a narrow pressure range centered at $50 - 70$ hPa. The zonal wind response consists mainly of an acceleration of the equatorward flanks of the tropospheric subtropical jets (Figure 9). The difference

between NOGAPS-ALPHA model runs for continuous warm and cold ENSO conditions at low latitudes also has characteristics that are very similar to the calculated tropical ENSO ozone and temperature regression coefficients (section 4; Figure 13; Table 1).

As discussed in section 5.1, when both the observational and model results are considered together, the pronounced cooling at $50 - 70$ hPa during warm events can be interpreted as primarily a radiative response to increased cloudiness in the upper troposphere. However, the negative ozone response and weaker cooling observed throughout the tropical lower stratosphere are attributable to an indirect dynamical effect, i.e., an acceleration of the Brewer-Dobson circulation, which is a result of enhanced Rossby wave activity associated with the tropical tropospheric circulation changes (see, e.g., Yulaeva et al., 1994; Garcia-Herrera et al., 2006; Deckert and Dameris, 2008; Randel et al., 2008]. As noted previously by Shibata and Deushi [2008], the observed zonal wind ENSO response can be interpreted as essentially a thermal wind response to increased latent heat release in the tropical troposphere. As discussed in section 5.2, the positive ozone response observed in the tropical middle stratosphere (centered near 10 hPa) is, by analogy to the ozone QBO, attributable to advective temperature and odd nitrogen decreases, which would lead to photochemical ozone increases.

In section 5.3, it was first noted that previous work has indicated that the tropical upwelling rate increases near or approaching solar minima [e.g., Kodera and Kuroda, 2002; Hood and Soukharev, 2003]. Such upwelling rate changes would lead to transport-induced ozone increases in the lower stratosphere near solar maxima, consistent with the observed total ozone variation (e.g., Figure 1b). It was then suggested that the observed insignificant ozone response to the solar cycle in the tropical middle stratosphere could

be a consequence of transport-induced increases in temperature and odd nitrogen mixing ratios (by analogy to those that occur in cold ENSO events). The latter would catalytically decrease the ozone mixing ratio, tending to cancel out the ozone increase resulting from direct solar UV-induced increases in ozone production.

Acknowledgments. We thank the three reviewers for detailed and useful comments. The Ozone Processing Team at Goddard Space Flight Center (led by R. Stolarski and R. McPeters) provided the Version 8 TOMS/SBUV(/2) column ozone and SBUV(/2) ozone profile data analyzed here. The SAGE II ozone profile monthly zonal means were provided by W. J. Randel and F. Wu of NCAR and were based on data originally obtained from the NASA Langley Research Center Radiation and Aerosols branch. The UARS HALOE data were obtained from the NASA Langley Research Center UARS data center (http://haloedata.larc.nasa.gov). We thank Ellis Remsberg for important advice and assistance in the acquisition and processing of the HALOE data. The ERA-40 zonal mean temperature and zonal wind data analyzed here were obtained from the European Center for Medium Range Weather Forecasting internet site. This work was supported in part by grants from the Office of Naval Research and from the National Aeronautics and Space Administration under Grant Nos. NNX06AC06G (L. Hood, P.I.) and NNH08AI67 (J. McCormack, P.I.) issued through the Living With a Star research TR&T program. NOGAPS-ALPHA simulations were made possible by a grant of computer time from the DoD High Performance Computing Modernization Program at the U.S. Air Force Research Laboratory.

References

Austin, J., K. Tourpali, E. Rozanov, H. Akiyoshi, S. Bekki, G. Bodeker, C. Brühl, N. Butchart, M. Chipperfield, M. Deushi, V. I. Fomichev, M. Giorgetta, L. Gray, K. Kodera, F. Lott, E. Manzini, D. Marsh, K. Matthes, T. Nagashima, K. Shibata, R. Stolarski, H. Struthers, and W. Tian, Coupled chemistry climate model simulations of the solar cycle in ozone and temperature, *J. Geophys. Res., 113*, D11306, doi:10.1029/2007JD009391, 2008.

Baldwin, M., L. Gray, T. Dunkerton, K. Hamilton, P. Haynes, W. Randel, J. Holton, M. J. Alexander, I. Hirota, T. Horinouchi, D. B. A. Jones, J. Kinnersley, C. Marquardt, K. Sato, and M. Takahashi (2001), The quasi-biennial oscillation, *Rev. Geophys., 39*, 179-229.

Bjerknes, J., A possible response of the atmospheric Hadley circulation to equatorial anomalies of ocean temperture (1966), *Tellus, 18*, 820-829.

Brönnimann, S. (2007) Impact of El Niño-Southern Oscillation on European climate, *Rev. Geophys., 45*, RG3003, doi:10.1029/2006RG000199.

Calvo, N., M. A. Giorgetta, R. Garcia-Herrera, and E. Manzini (2009), Nonlinearity of the combined warm ENSO and QBO effects on the Northern Hemisphere polar vortex in Maecham5 simulations, *J. Geophys. Res., 114*, D13, doi:10.1029/2008JD011445.

Calvo-Fernandez, N., R. Garcia, R. Garcia-Herrera, D. Puyol, L. Gimeno Presa, E. Hernandez-Martin, and P. Ribera Rodriguez (2004), Analysis of the ENSO signal in tropospheric and stratospheric temperatures observed by MSU, 1979-2000, *J. Climate, 17*, 3934-3946.

Chandra, S., and R. D. McPeters (1994), The solar cycle variation of ozone in the stratosphere inferred from Nimbus 7 and NOAA 11 satellites, *J. Geophys. Res., 99*, 20,665-20,671.

Chipperfield, M. P., L. J. Gray, J. S. Kinnersley, and J. Zawodny (1994), A two-dimensional model study of the QBO signal in SAGE II NO_2 and O_3, *Geophys. Res. Lett., 21*, 589-592, 1994.

Chou, M.-D., and M. J. Suarez (2002), A solar radiation parameterization for atmospheric studies, NASA Tech. Mem. 10460, 15, *Technical Report Series on Global Modeling and Data Assimilation*, edited by Suarez, M. J., 52pp.

Chou, M.-D., M. J. Suarez, X. Z. Liang, and M.-H. Yan, (2001), A thermal infrared radiation parameterization for atmospheric studies, NASA Tech. Mem. 104606, 19, *Technical Report Series on Global Modeling and Data Assimilation*, edited by Suarez, M. J., 65pp.

Crooks, S., and L. Gray, Characterization of the 11-year solar signal using a multiple regression analysis of the ERA-40 Dataset, *J. Climate, 18*, 996-1015, 2005.

Deckert, R., and M. Dameris (2008), Higher tropical SSTs strengthen the tropical upwelling via deep convection, *Geophys. Res. Lett., 35*, L10813, doi:10.1029/2008GL033719.

Eckermann, S. D. (2009), Hybrid σ–p coordinate choices for a global model, *Mon. Wea. Rev., 137*, 224–245.

Eckermann, S. D., K. W, Hoppel, L. Coy,, J. P. McCormack, D. E. Siskind, K. Nielsen, A. Kochenash, M. H. Stevens, and C. R. Englert (2008), High-altitude data assimilation system experiments for the Northern Hemisphere summer mesosphere season of 2007, *J. Atmos. Sol. Terr. Phys.*, doi:10.1016/j.jastp.2008.09.036.

Fomichev, V., J.-P. Blanchet, and D. Turner (1998), Matrix parameterization of the 15 μm CO_2 band cooling in the middle and upper atmosphere for variable CO_2 concentration, *J. Geophys. Res., 103*(D10), 11505-11528.

Free, M., and D. J. Seidel (2009), Observed El Niño-Southern Oscillation temperature signal in the stratosphere, *J. Geophys. Res., 114*, D23108, doi:10.1029/2009JD012420.

Frith, S. M., and R. S. Stolarski (2005), Merged profile ozone data from the SBUV/SBUV2 series of instruments, Abstract A23B-0943, Fall AGU Meeting, San Francisco, California, December, 2005, American Geophysical Union, Washington, D. C.

Garcia, R. R., D. R. Marsh, D. E. Kinnison, B. A. Boville, and F. Sassi (2007), Simulation of secular trends in the middle atmosphere, *J. Geophys. Res., 112*, D09301, doi:10.1029/2006JD007485.

Garcia-Herrera, R., N. Calvo, R. R. Garcia, and M. A. Giorgetta (2006), Propagation of ENSO temperature signals into the middle atmosphere: A comparison of two general circulation models and ERA-40 reanalysis data, *J. Geophys. Res., 111*, D06101, doi:10.1029/2005JD006061.

Garfinkel, C. I., and D. L. Hartmann (2007), Effects of the El Niño-Southern Oscillation and the Quasi-Biennial Oscillation on polar temperatures in the stratosphere, *J. Geophys. Res., 112*, D19112, doi:10.1029/2007JD008481.

Gray, L. J., S. A. Crooks, M. A. Palmer, C. L. Pascoe, and S. Sparrow (2006) A possible transfer mechanism for the 11-year solar cycle to the lower stratosphere, *Space Sci. Rev., 125*, 357-370.

Gray, L. J., S. T. Rumbold, and K. P. Shine (2009) Stratospheric temperature and radiative forcing response to 11-year solar cycle changes in irradiance and ozone, *J. Atmos.*

Sci., 66, 2402-2417.

Gray, L. J., J. Beer, M. Geller, J. Haigh, M. Lockwood, K. Matthes, U. Cubasch, D. Fleitmann, G. Harrison, L. Hood, J. Luterbacher, G. Meehl, D. Shindell, B. van Geel, and W. White (2010), Solar influences on climate, *Rev. Geophys.* submitted.

Hasebe, F. (1983), Interannual variations of global total ozone revealed from Nimbus 4 BUV and ground-based observations, *J. Geophys. Res., 88*, 6819-6834.

Hood, L. L. (1997), The Solar cycle variation of total ozone: Dynamical forcing in the lower stratosphere, *J. Geophys. Res., 102*, 1355-1370, 1997.

Hood L. L. (2004), Effects of solar UV variability on the stratosphere, in *Solar Variability and Its Effect on the Earth's Atmospheric and Climate System, AGU Geophys. Monogr. Ser.*, edited by J. Pap, P. Fox, C. Frohlich, H. Hudson, J. Kuhn, J. McCormack, G. North, W. Sprigg, and S. T. Wu, American Geophysical Union, Washington, D. C., p. 283-304.

Hood, L. L., J. L. Jirikowic, and J. P. McCormack (1993), Quasi-decadal variability of the stratosphere: Influence of long-term solar ultraviolet variations, *J. Atmos. Sci., 50*, 3941-3957.

Hood, L. L. and J. P. McCormack (1992), Components of interannual ozone change based on Nimbus 7 TOMS data, *Geophys. Res. Lett., 19*, 2309-2312.

Hood, L. L., and B. E. Soukharev (2003), Quasi-decadal variability of the tropical lower stratosphere: The role of extratropical wave forcing, *J. Atmos. Sci., 60*, 2389-2403.

Hoppel, K. W., N. L. Baker, L. Coy, S. D. Eckermann, J. P. McCormack, G. Nedoluha, G., and D. E. Siskind (2008), Assimilation of stratospheric and mesospheric temperatures from MLS and SABER in a global NWP model, *Atmos. Chem. Phys. Discuss., 8*,

8455–8490.

Ito, K., Y. Naito, and S. Yoden (2009), Combined effects of QBO and 11-year solar cycle on the winter hemisphere in a stratosphere-troposphere coupled system, *Geophys. Res. Lett., 36*, L11804, doi:10.1029/2008GL037117.

Kodera, K., and Y. Kuroda (2002), Dynamical response to the solar cycle: Winter stratopause and lower stratosphere, *J. Geophys. Res., 101*, 4749, doi:10.1029/2002JD002224.

Labitzke, K. (2004), On the signal of the 11-year sunspot cycle in the stratosphere and its modulation by the quasi-biennial oscillation, *J. Atmos. Solar Terr. Phys., 66*, 1151-1157.

Lee, H., and A. K. Smith (2003), Simulation of the combined effects of solar cycle, quasi-biennial oscillation, and volcanic forcing on stratospheric ozone changes in recent decades, *J. Geophys. Res., 108*(D2), 4049, doi:10.1029/2001JD001503.

Marsh, D. R., and R. R. Garcia (2007), Attribution of decadal variability in lower-stratospheric tropical ozone, *Geophys. Res. Lett., 34*, L21807, doi:10.1029/2007GL030935.

Matthes, K., Y. Kuroda, K. Kodera, and U. Langematz (2006), Transfer of the solar signal from the stratosphere to the troposphere: Northern winter, *J. Geophys. Res., 111*, D06108, doi:10.1029/2005JD006283.

Matthes, K., U. Langematz, L. J. Gray, K. Kodera, and K. Labitzke (2004), Improved 11-year solar signal in the Freie Universität Berlin climate middle atmosphere model (FUB-CMAM), *J. Geophys. Res., 109*, D06101, doi:10.1029/2003JD004012.

Matthes, K., K. Kodera, L. Gray, J. Austin, A. Kubin, U. Langematz, D. Marsh, J. McCormack, K. Shibata, and D. Shindell (2007), Report on the first SOLARIS workshop

4-6 October 2006, Boulder, Colorado, USA, *SPARC Newsletter, 28*.

McCormack, J. P., and L. L. Hood (1996), Apparent solar cycle variations of upper stratospheric ozone and temperature: Latitude and seasonal dependences, *J. Geophys. Res., 101*, 20,933-20,944.

McCormack, J. P., S. D. Eckermann, D. Siskind, and T. McGee (2006), CHEM2D-OPP: A new linearized gas-phase ozone photochemistry parameterization for high-altitude NWP and climate models, *Atmos. Chem. Phys., 6*, 4943-4972.

McCormack, J. P., D. E. Siskind, and L. L. Hood (2007), Solar-QBO interaction and its impact on stratospheric ozone in a zonally averaged photochemical transport model of the middle atmosphere, *J. Geophys. Res., 112*, D16109, doi:10.1029/2006JD008369.

McCormack, J. P., K. H. Hoppel, and D. S. Siskind (2008), Parameterization of middle atmospheric water vapor photochemistry for high-altitude NWP and data assimilation, *Atmos. Chem. Phys. Discuss., 8*, 13,999–14032, 2008.

Meehl, G. A., W. M. Washington, T. M. L. Wigley, J. M. Arblaster, and A. Dai (2003), Solar and greenhouse gas forcing and climate response in the 20th century, *J. Climate, 16*, 426-444.

Meehl, G. A., J. M. Arblaster, K. Matthes, F. Sassi, and H. van Loon (2009) Amplifying the Pacific climate system response to a small 11-year solar cycle forcing, *Science, 325*, 1114-1118.

Neter, J., W. Wasserman, and M. H. Kutner, *Applied Linear Regression Models*, R. D. Irwin, Inc., 1985.

Randel, W. J., and J. B. Cobb (1994), Coherent variations of monthly mean total ozone and lower stratospheric temperature, *J. Geophys. Res., 99*, 5433-5447.

Randel, W. J., and F. Wu (1996), Isolation of the ozone QBO in SAGE II data by singular-value decomposition, 2546-2559.

Randel, W. J., and F. Wu (2007), A stratospheric ozone profile data set for 1979-2005; Variability, trends, and comparisons with column ozone data, *J. Geophys. Res., 112*, D06313, doi:10.1029/2006JD007339.

Randel, W. J., R. Garcia, and F. Wu (2008) Dynamical balances and tropical stratospheric upwelling, *J. Atmos. Sci., 65*, 3584-3595.

Randel, W. J., K. Shine, J. Austin, J. Barnett, C. Claud, N. Gillett, P. Keckhut, U. Langematz, R. Lin, C. Long, C. Mears, A. Miller, J. Nash, D. Seidel, D. W. J. Thompson, F. Wu, and S. Yoden (2009a), An update of observed stratospheric temperature trends, *J. Geophys. Res., 114*, D02107, doi:10.1029/2008JD010421.

Randel, W. J., R. R. Garcia, N. Calvo, and D. Marsh (2009b), ENSO influence on zonal mean temperature and ozone in the tropical lower stratosphere, *Geophys. Res. Lett., 36*, L15822, doi:10.1029/2009GL039343.

Reid, G. C. (1994), Seasonal and interannual temperature variations in the tropical stratosphere, *J. Geophys. Res., 99*, 18923-18932.

Reid, G. C., K. S. Gage, and J. R. McAfee (1989), The thermal response of the tropical atmosphere to variations in equatorial Pacific sea surface temperature, *J. Geophys. Res., 94*, 14705-14716.

Reinsel, G. C., A. J. Miller, E. C. Weatherhead, L. E. Flynn, R. M. Nagatani, G. C. Tiao, and D. J. Wuebbles (2005), Trend analysis of total ozone data for turnaround and dynamical contributions, *J. Geophys. Res., 110*, D16306, doi:10.1029/2004JD004662.

Robock, A. (2000), Volcanic eruptions and climate, *Rev. Geophys., 38*, 191-219.

Salby, M. L., and P. F. Callaghan (2006), Evidence of the solar cycle in the tropical troposphere, *J. Geophys. Res., 111*, D21113, doi:10.1029/2006JD007133.

Shibata, K., and M. Deushi (2008), Long-term variations and trends in the simulation of the middle atmosphere 1980-2004 by the chemistry-climate model of the Meteorological Research Institute, *Ann. Geophys., 26*, 1299-1326.

Shiotani, M. (1992), Annual, quasi-biennial, and El Niño-Southern Oscillation (ENSO) time scale variations in equatorial total ozone, *J. Geophys. Res., 97*, 7625-7633.

Solomon, S., R. W. Portmann, R. R. Garcia, L. W. Thomason, L. R. Poole, and M. P. McCormick (1996), The role of aerosol variations in anthropogenic ozone depletion at northern midlatitudes, *J. Geophys. Res., 101*, 6713-6728.

Soukharev, B. E., and L. Hood (2006), Solar cycle variation of stratospheric ozone: Multiple regression analysis of long-term satellite data sets and comparisons with models, *J. Geophys. Res., 111*, D20314, doi:10.1029/2006JD007107.

Steinbrecht, W., B. Hassler, H. Claude, P. Winkler, and R. S. Stolarski (2003), Global distribution of total ozone and lower stratospheric temperature variations, *Atmos. Chem. Phys., 3*, 1421-1438.

Stenchikov, G., A. Robock, V. Ramaswamy, M. D. Schwarzkopf, K. Hamilton, and S. Ramachandran (2002), Arctic Oscillation response to the 1991 Mount Pinatubo eruption: Effects of volcanic aerosols and ozone depletion, *J. Geophys. Res., 107*(D24), 4803, doi:10.1029/2002JD002090.

Stolarski, R. S., P. Bloomfield, R. D. McPeters, and J. R. Herman (1991), Total ozone trends deduced from Nimbus 7 TOMS data, *Geophys. Res. Lett., 18*, 1015-1018.

Thomason, L. W., L. R. Poole, and T. Deshler (1997), A global climatology of stratospheric aerosol surface area density deduced from Stratospheric Aerosol and Gas Experiment II measurements: 1984-1994, *J. Geophys. Res., 102*(D7), 8967-8976.

Tourpali, K., C. S. Zerefos, D. S. Balis, and A. F. Bais (2007), The 11-year solar cycle in stratospheric ozone: Comparison between Umkehr and SBUVv8 and effects on surface erythemal irradiance, *J. Geophys. Res., 112*, D12306, doi:10.1029/2006JD007760.

van Loon, H., G. Meehl, and D. Shea (2007), Coupled air-sea response to solar forcing in the Pacific region during northern winter, *J. Geophys. Res., 112*, D02108, doi:10.1029/2006JD007378.

van Loon, H., and G. A. Meehl (2008) The response in the Pacific to the Sun's decadal peaks and contrasts to cold events in the Southern Oscillation, *J. Atmos. Solar Terr. Phys., 70*, 1046-1055.

Viereck, R., and L. Puga (1999), The NOAA MG II core-to-wing solar index: Construction of a 20-year time series of chromospheric variability from multiple satellites, *J. Geophys. Res., 104*, 9995-10005.

Wang, H. J., D. M. Cunnold, and X. Bao (1996), A critical analysis of SAGE ozone trends, *J. Geophys. Res., 101*, 12,495-12,514.

Webster, P. J., and G. L. Stephens, Tropical upper tropospheric extended clouds: Inferences from winter MONEX (1980) *J. Atmos. Sci., 37*, 1521-1541.

Webster, S., A. R. Brown, D. R. Cameron, and C. P. Jones (2003), Improvements to the representation of orography in the Met Office Unified Model, *Q. J. Roy. Meteorol. Soc., 129*, 1989–2010.

White, W., and Z. Liu (2008), Resonant excitation of the quasi-decadal oscillation by the 11-year signal in the Sun's irradiance, *J. Geophys. Res., 113*, C01002, doi:10.1029/2006JC004057.

World Meteorological Organization (WMO) (2007), Scientific Assessment of Ozone Depletion: 2006, World Meteorological Organization, Global Ozone Research and Monitoring Project, Report No. 50.

Yulaeva, E., and J. M. Wallace (1994), The signature of ENSO in global temperature and precipitation fields derived from the Microwave Sounding Unit, *J. Climate, 7*, 1719-1736.

Yulaeva, E., J. R. Holton, and J. M. Wallace (1994), On the cause of the annual cycle in tropical lower-stratospheric temperatures, *J. Atmos. Sci., 51*, 169-174, 1994.

Zerefos, C. W., K. Tourpali, B. R. Bojkov, D. S. Balis, B. Rognerund, and I. S. A. Isaksen (1997) Solar activity-total ozone relationships: Observations and model studies with heterogeneous chemistry, *J. Geophys. Res., 102*, 1561-1569.

Figure 1. Comparisons of the solar Mg II UV index with area-weighted averages over two latitude ranges of the monthly mean version 8 TOMS/SBUV(/2) total ozone anomaly. Also indicated are the times of the El Chichón (C) and Pinatubo (P) volcanic eruptions.

Figure 2. Comparison of the Niño 3.4 index with the TOMS/SBUV(/2) total ozone anomaly averaged over tropical latitudes. Also indicated are the correlation coefficients (R) at zero lag and at 4 months lag (the lag at which $|R|$ maximizes).

Figure 3. Comparison of annual mean solar cycle ozone regression coefficients calculated from SBUV(/2) data (a) using the regression model (1) without an ENSO term and (b) using the regression model (1) with an ENSO term at optimum lag. The contour interval is 0.5% and shaded areas are significant at 95% confidence.

Figure 4. Comparison of tropically averaged solar cycle ozone regression coefficients calculated from the three satellite data sets analyzed by Soukharev and Hood [2006] (top panel) using the regression model (1) without an ENSO term and (bottom panel) using the regression model (1) with an ENSO term at optimum lag.

Figure 5. Same format as Figure 3 but for boreal winter (December, January, February) solar cycle ozone regression coefficients.

Figure 6. Comparison of solar cycle column ozone regression coefficients for boreal winter (DJF) calculated from Version 8 TOMS/SBUV data (a) using the regression model (1) without an ENSO term and (b) using the model (1) with an ENSO term at optimum lag.

Figure 7. Per cent change in version 8 SBUV(/2) ozone for a 1 unit change of the Niño 3.4 index. Shaded areas are significant at the 95% confidence level.

Figure 8. Same format as Figure 7 but for (a) SAGE II ozone profile data over the 1985-2003 period and (b) UARS HALOE ozone profile data over the 1992-2003 period.

Figure 9. Annual mean ENSO regression coefficients from ERA-40 data for (a) temperature in Kelvin per unit of N3.4; and (b) zonal mean zonal wind in m/s per unit of N3.4. Shaded areas are significant at the 95% confidence level.

Figure 10. Same format as Figure 7 but for annual mean version 8 TOMS/SBUV(/2) column ozone data as a function of latitude and longitude.

Figure 11. Seasonal dependence of the TOMS/SBUV(/2) total ozone ENSO regression coefficient. From top to bottom: Winter (DJF), Spring (MAM), Summer (JJA), Fall (SON). Shaded areas are significant at 95% confidence level.

Figure 12. Comparison of the Niño 3.4 ENSO index for the two northern winter periods for which simulations were performed using the NOGAPS-ALPHA model.

Figure 13. Difference between the NOGAPS-ALPHA ensemble model runs for warm (DJF03) and cold (DJF08) ENSO conditions as a function of time (days), averaged over the 10°S to 10°N latitude range, for (a) ozone mixing ratio (C.I. = 0.05 ppmv); (b) temperature (C.I. = 0.5 Kelvin); and (c) zonally averaged vertical velocity (contours at ±0.1, ±0.2, ±0.4, ±0.8, ±1.2 ... mm/s). Blue and red colors indicate negative and positive values, respectively. All values should be divided by ~ 3 to convert to units per unit of N3.4.

Figure 14. Same as Figure 13a but plotted in units of per cent (contours at ±1, ±2, ±3, ±4, ±5, ±10, and ±20%). Values should again be divided by ~ 3 to convert to per cent per unit of N3.4.

Figure 15. Comparison of 3-month zonal averages of UARS HALOE sunset measurements at 10 hPa, 5°S to 5°N, of (a) NO + NO_2; and (b) O_3 over the 1992 to 2003 period.

Table 1. Mean O_3 Concentration and ENSO O_3 Regression Coefficients, 24°S - 24°N, 1979-2003

P	$[O_3]^*$	SBUV	SAGE II	HALOE	WACCM**	NOGAPS†
hPa	DU/km	%/N3.4	%/N3.4	%/N3.4	%/N3.4	%/N3.4
20	17.7	−0.69	−0.37	−0.68	−0.5	−0.5
30	15.8	−0.86	−0.50	−0.72	−1.5	−0.6
40	13.0	−0.85	−0.57	−0.47	−2.2	−0.8
50	9.6	−0.75	−1.25	−0.16	−2.8	−1.2
70	3.4	–	−3.32	−1.63	−3.3	−4.2

* Approximate long-term means from SAGE II data

** From Figure 4 of Marsh and Garcia [2007]

† Estimated from mean differences over the last 60 days of the integrations

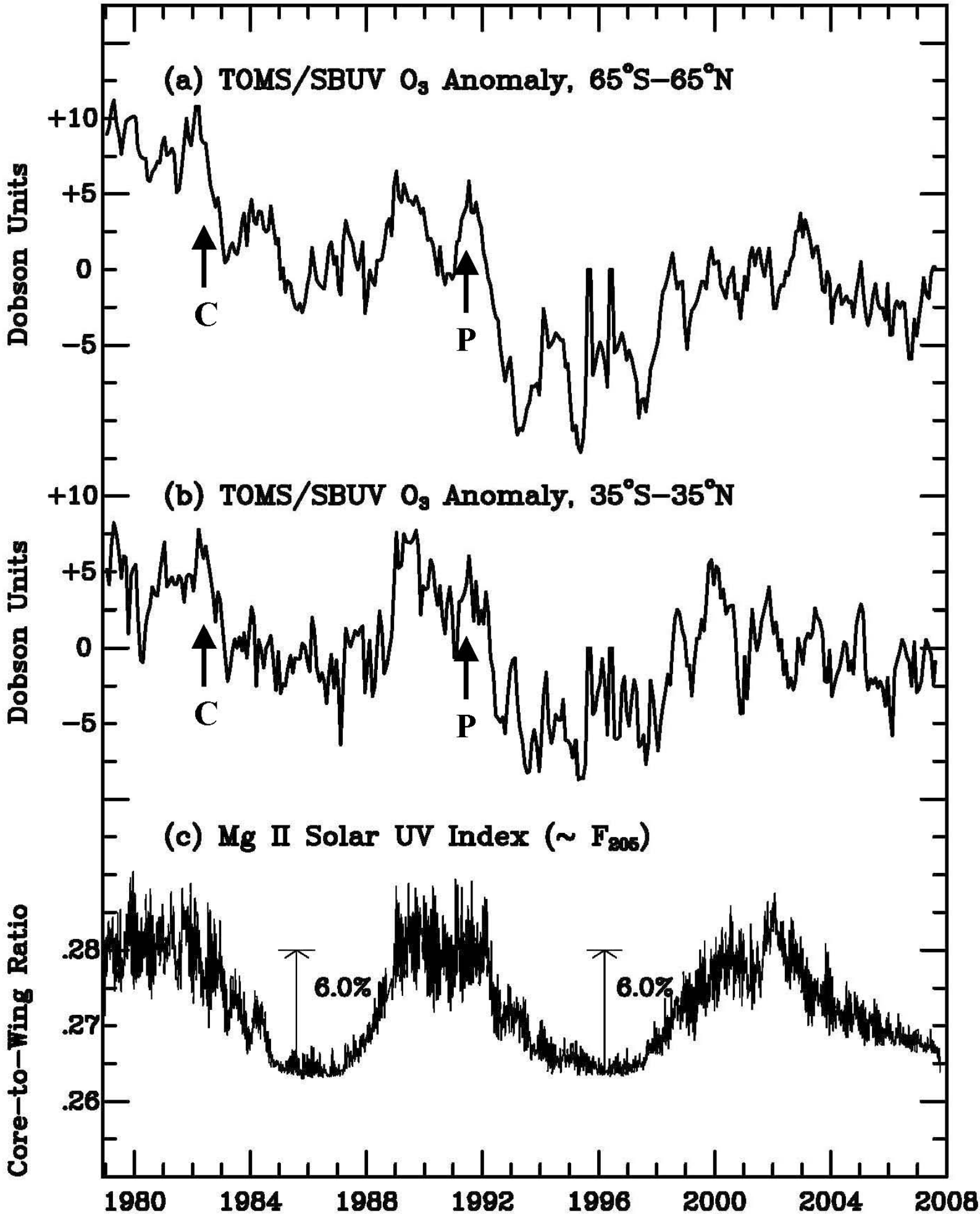
(a) TOMS/SBUV O_3 Anomaly, 65°S–65°N
Dobson Units
+10
+5
0
−5
C
P
(b) TOMS/SBUV O_3 Anomaly, 35°S–35°N
Dobson Units
+10
+5
0
−5
C
P
(c) Mg II Solar UV Index (~ F_{205})
Core–to–Wing Ratio
.28
.27
.26
6.0%
6.0%
1980
1984
1988
1992
1996
2000
2004
2008

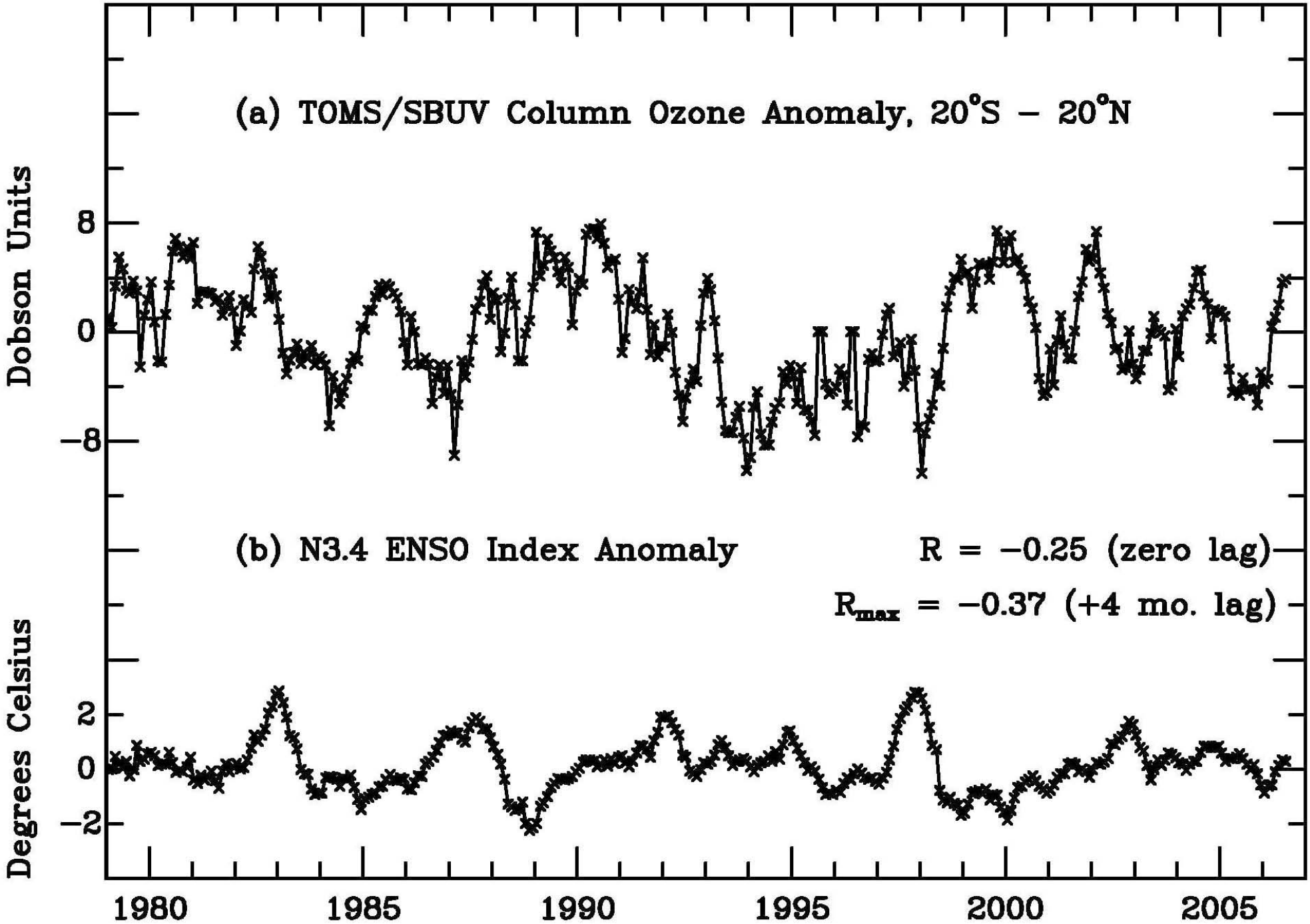
(a) TOMS/SBUV Column Ozone Anomaly, 20°S – 20°N
Dobson Units
8
0
−8
(b) N3.4 ENSO Index Anomaly
R = −0.25 (zero lag)
R_{max} = −0.37 (+4 mo. lag)
Degrees Celsius
2
0
−2
1980
1985
1990
1995
2000
2005

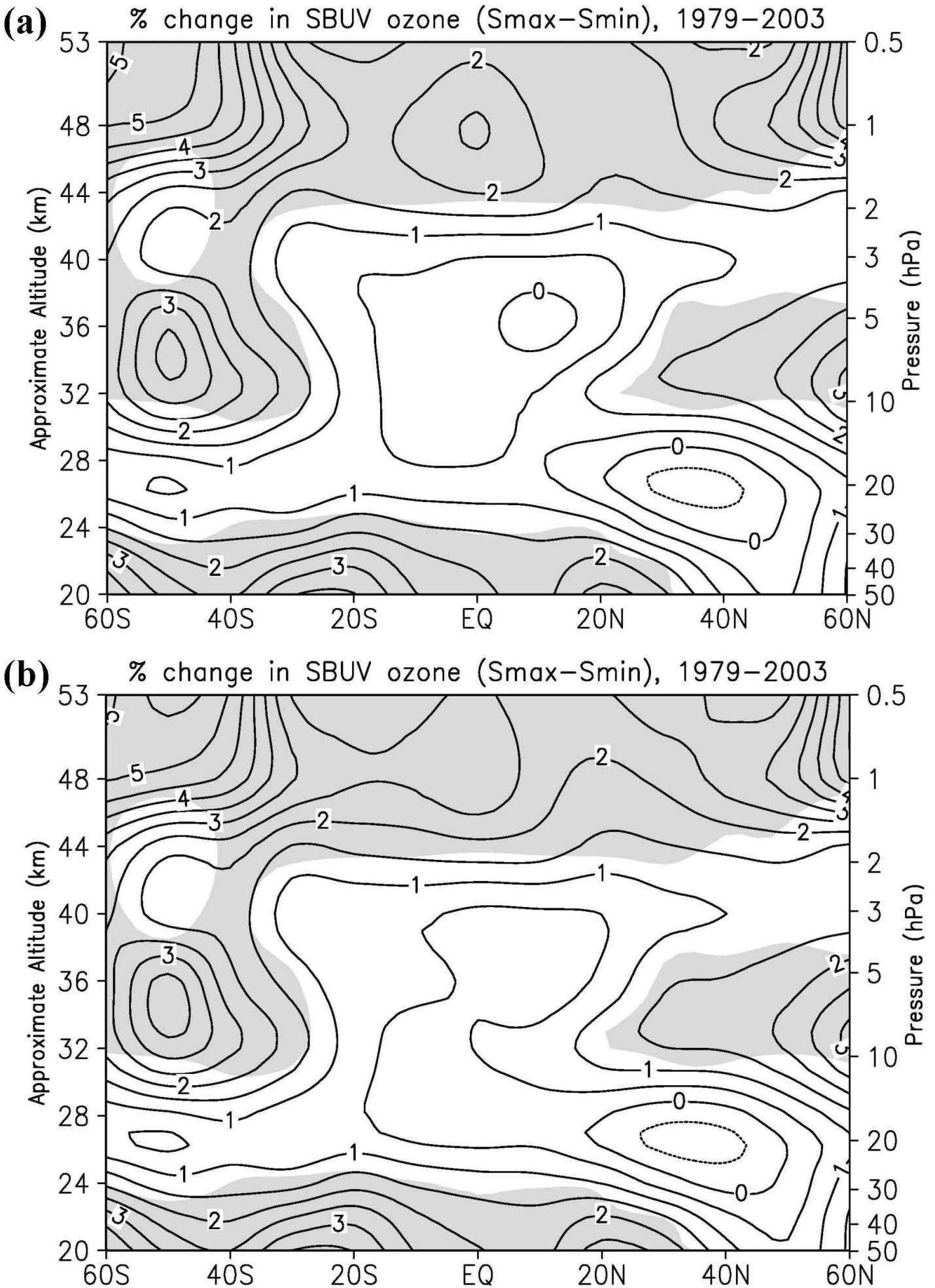
(a)
% change in SBUV ozone (Smax−Smin), 1979−2003
Approximate Altitude (km)
Pressure (hPa)
53
48
44
40
36
32
28
24
20
0.5
1
2
3
5
10
20
30
40
50
60S
40S
20S
EQ
20N
40N
60N
(b)
% change in SBUV ozone (Smax−Smin), 1979−2003
Approximate Altitude (km)
Pressure (hPa)
60S
40S
20S
EQ
20N
40N
60N

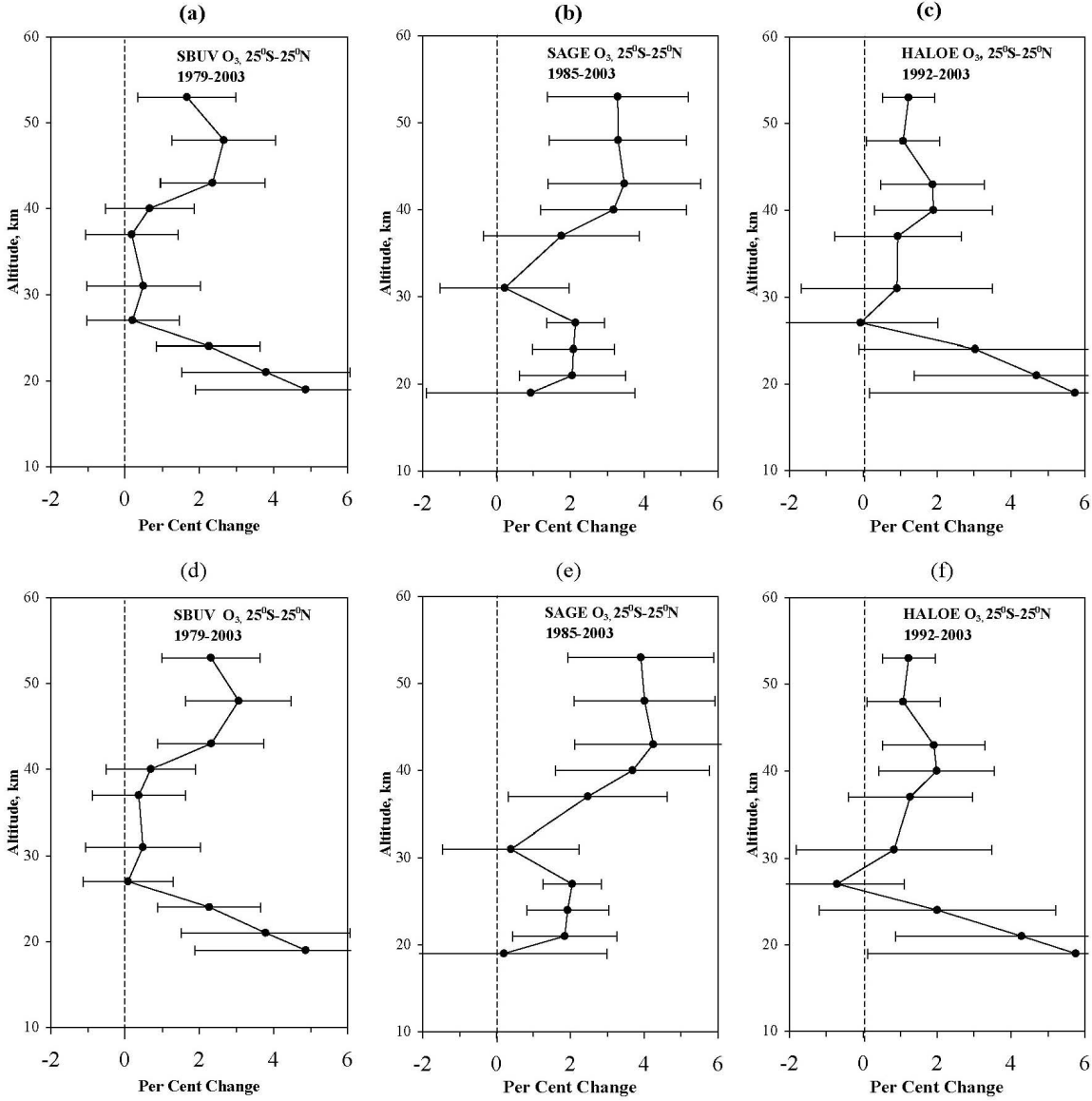
(a)
SBUV O_3, 25°S-25°N
1979-2003
(b)
SAGE O_3, 25°S-25°N
1985-2003
(c)
HALOE O_3, 25°S-25°N
1992-2003
(d)
SBUV O_3, 25°S-25°N
1979-2003
(e)
SAGE O_3, 25°S-25°N
1985-2003
(f)
HALOE O_3, 25°S-25°N
1992-2003
Altitude, km
Per Cent Change
60
50
40
30
20
10
-2
0
2
4
6

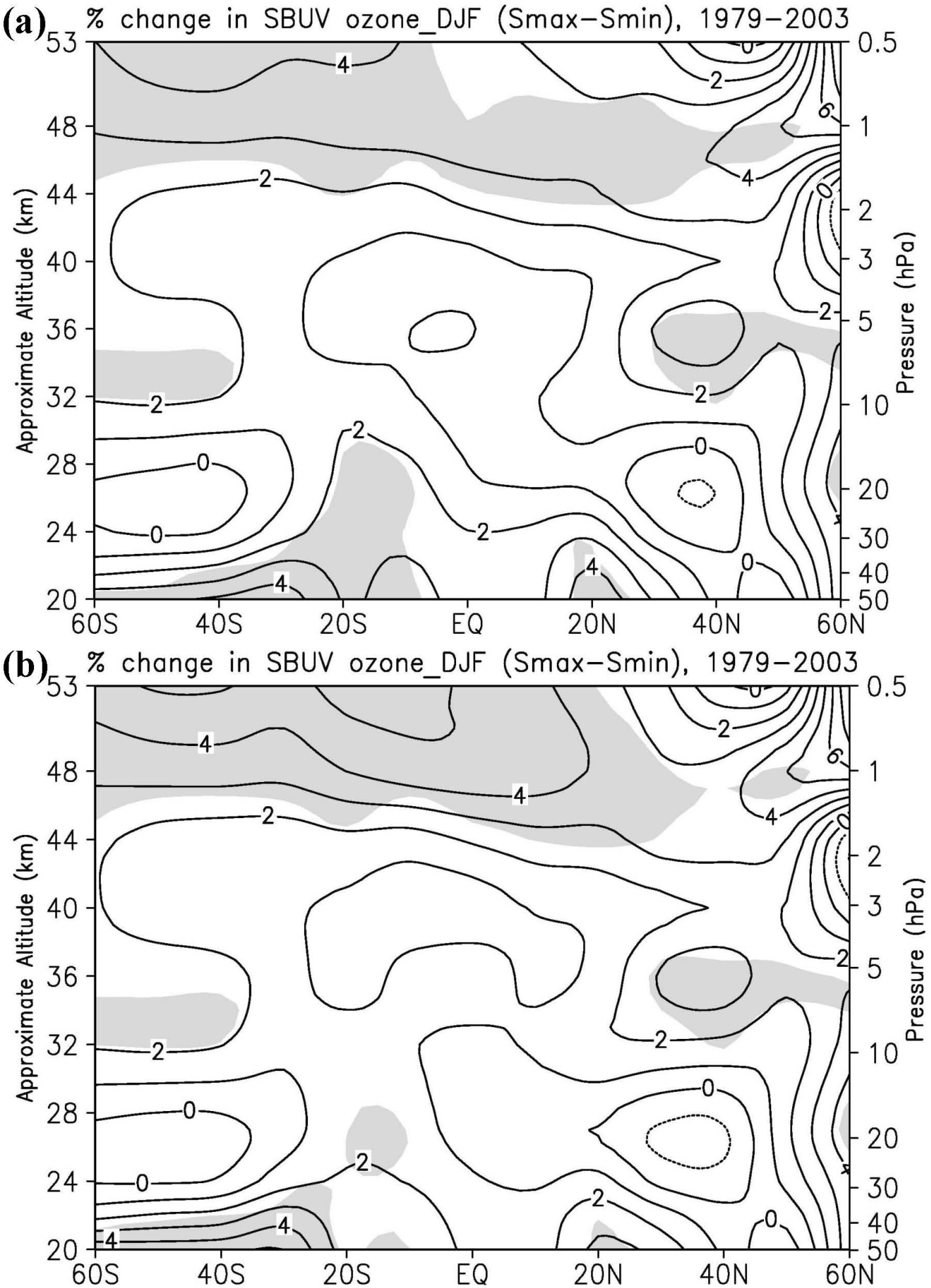
(a)
% change in SBUV ozone_DJF (Smax−Smin), 1979−2003
Approximate Altitude (km)
Pressure (hPa)
53
48
44
40
36
32
28
24
20
0.5
1
2
3
5
10
20
30
40
50
60S
40S
20S
EQ
20N
40N
60N
(b)
% change in SBUV ozone_DJF (Smax−Smin), 1979−2003
Approximate Altitude (km)
Pressure (hPa)
60S
40S
20S
EQ
20N
40N
60N

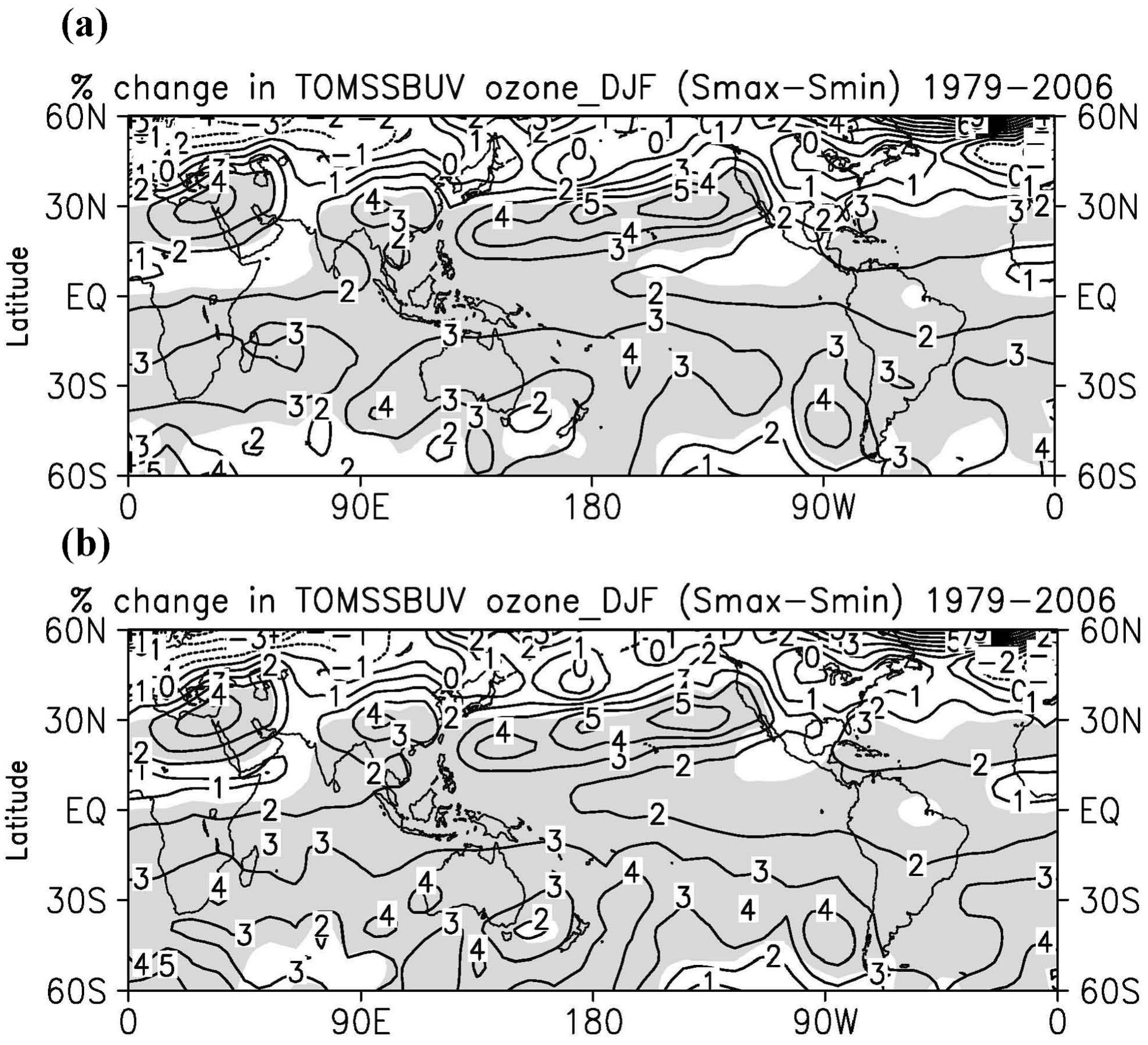
(a)
% change in TOMSSBUV ozone_DJF (Smax−Smin) 1979−2006
60N
30N
EQ
30S
60S
Latitude
0
90E
180
90W
0
(b)
% change in TOMSSBUV ozone_DJF (Smax−Smin) 1979−2006
60N
30N
EQ
30S
60S
Latitude
0
90E
180
90W
0

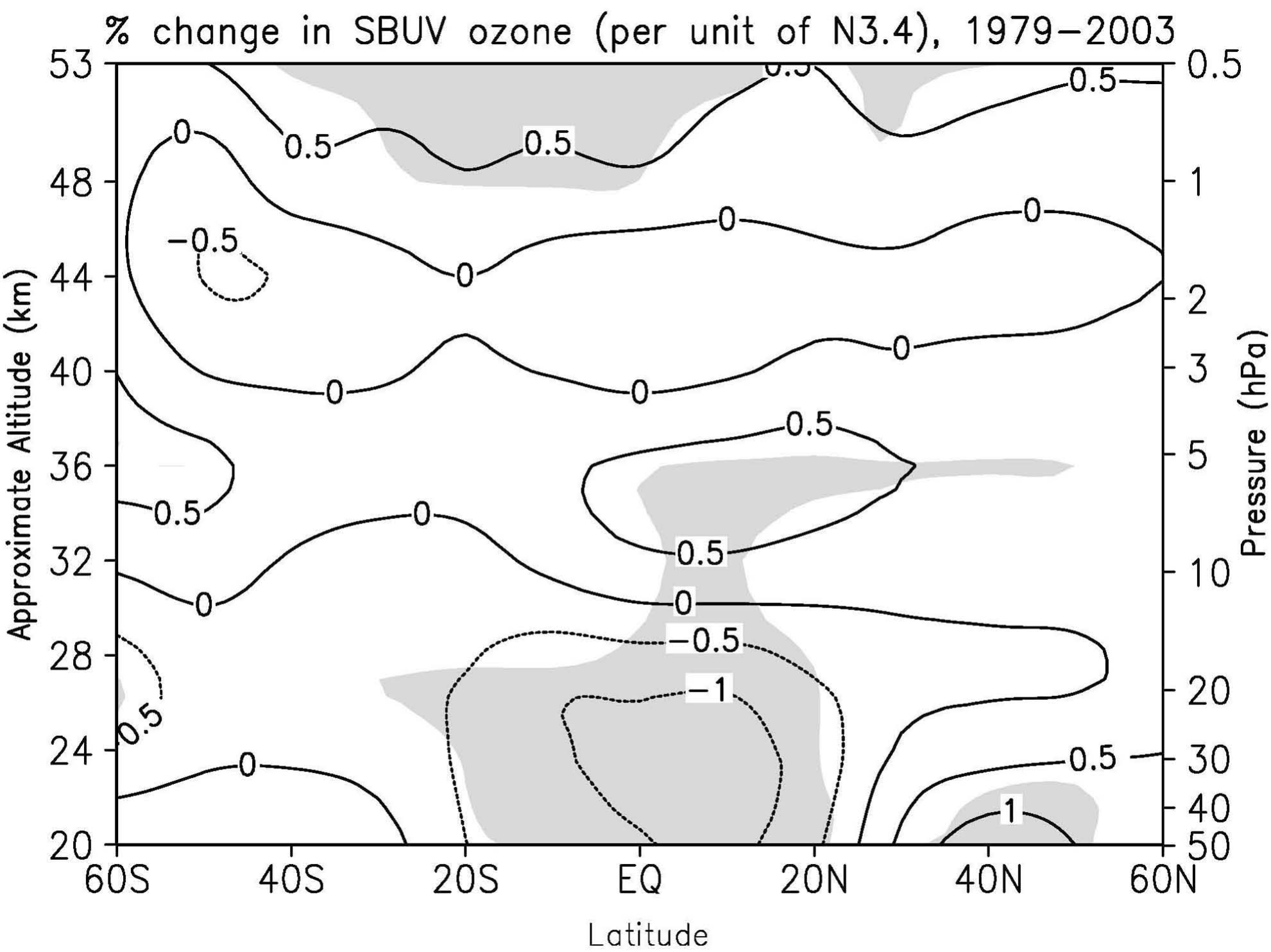
% change in SBUV ozone (per unit of N3.4), 1979–2003
Approximate Altitude (km)
53
48
44
40
36
32
28
24
20
Pressure (hPa)
0.5
1
2
3
5
10
20
30
40
50
60S
40S
20S
EQ
20N
40N
60N
Latitude
0.5
0
−0.5
−1
1

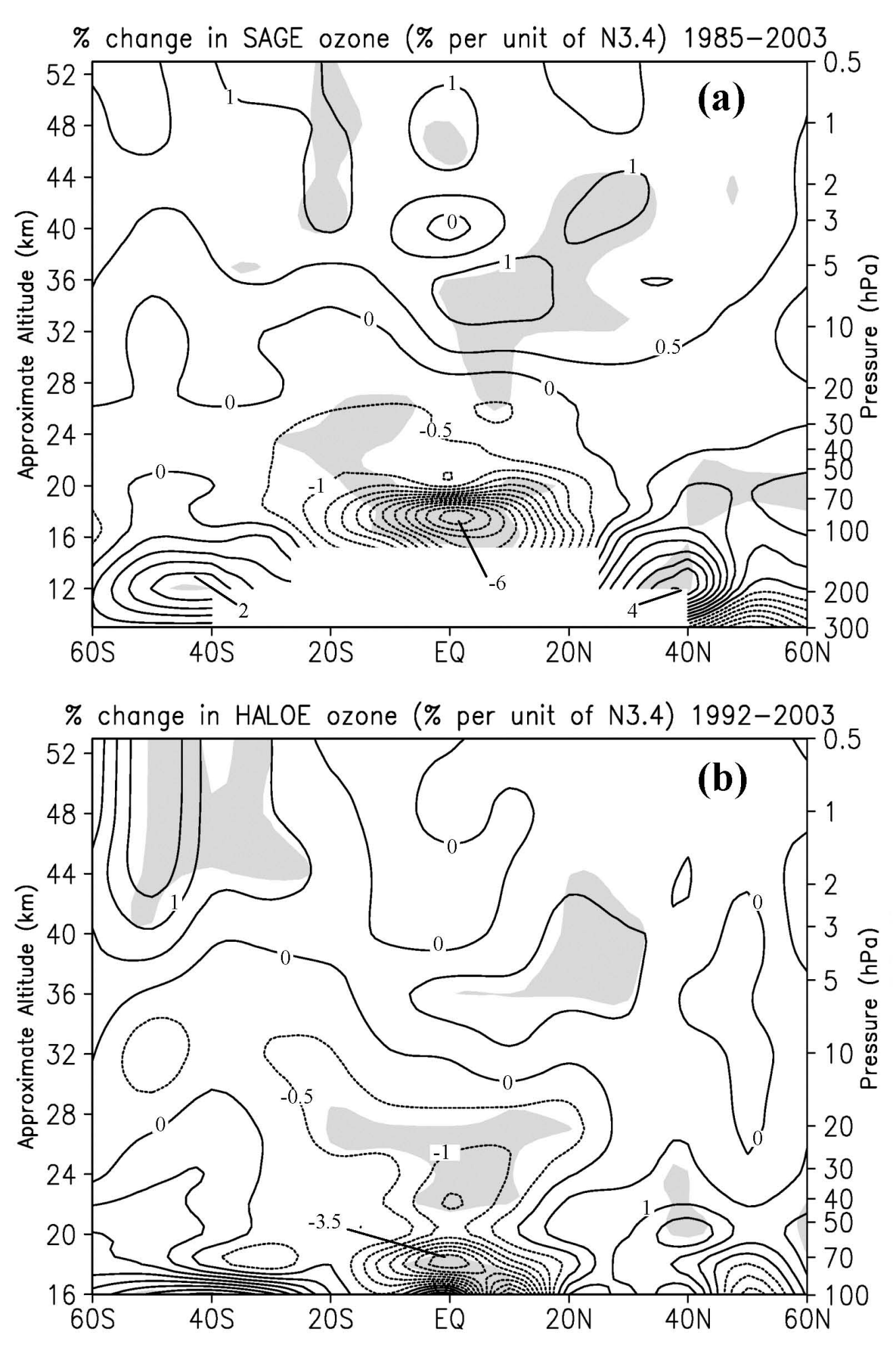
% change in SAGE ozone (% per unit of N3.4) 1985–2003
(a)
Approximate Altitude (km)
Pressure (hPa)
52
48
44
40
36
32
28
24
20
16
12
0.5
1
2
3
5
10
20
30
40
50
70
100
200
300
1
0
0.5
-0.5
-1
-6
2
4
60S
40S
20S
EQ
20N
40N
60N
% change in HALOE ozone (% per unit of N3.4) 1992–2003
(b)
Approximate Altitude (km)
Pressure (hPa)
52
48
44
40
36
32
28
24
20
16
0.5
1
2
3
5
10
20
30
40
50
70
100
1
0
-0.5
-1
-3.5
60S
40S
20S
EQ
20N
40N
60N

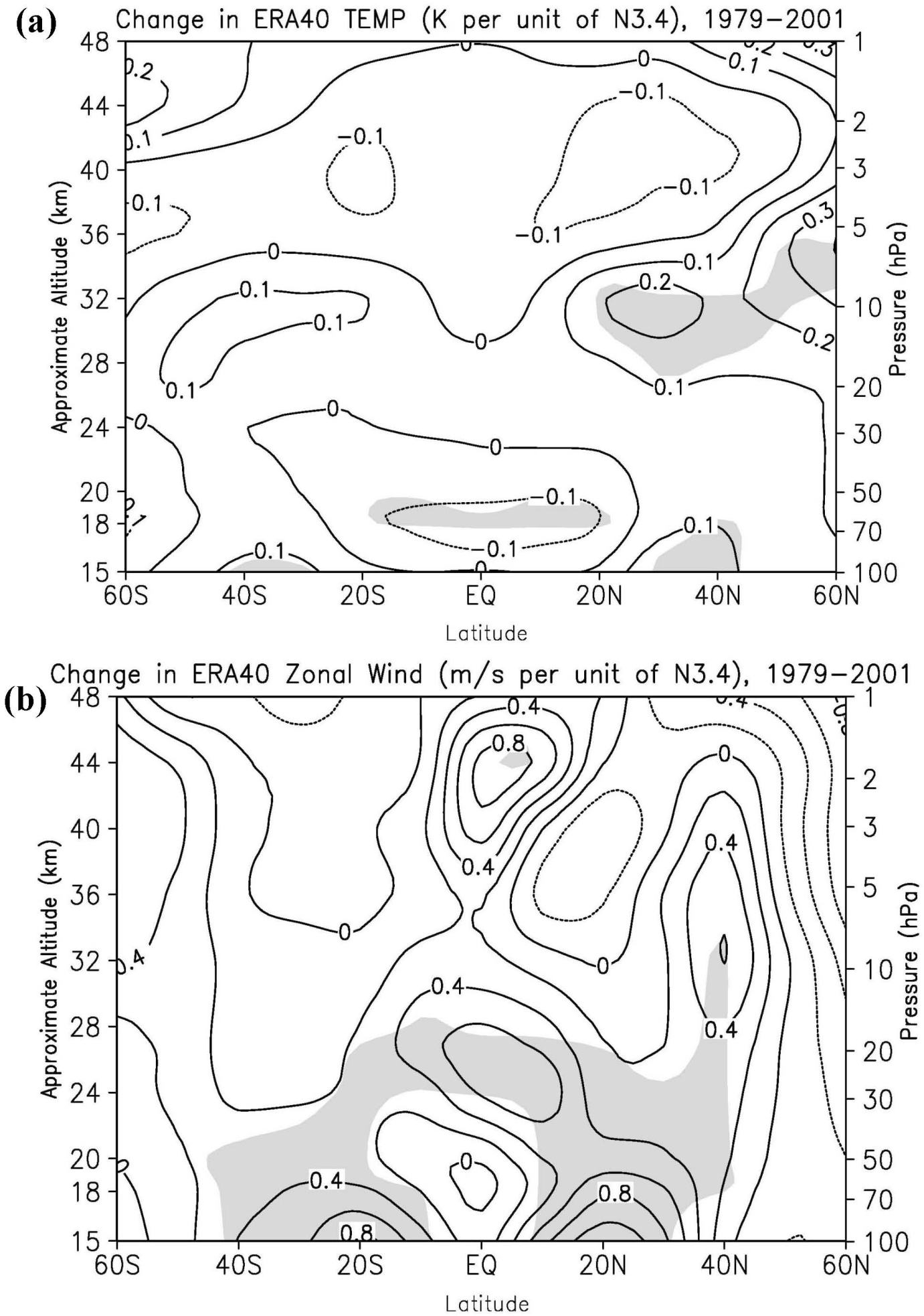
(a)
Change in ERA40 TEMP (K per unit of N3.4), 1979–2001
Approximate Altitude (km)
Pressure (hPa)
Latitude
60S
40S
20S
EQ
20N
40N
60N
(b)
Change in ERA40 Zonal Wind (m/s per unit of N3.4), 1979–2001
Approximate Altitude (km)
Pressure (hPa)
Latitude
60S
40S
20S
EQ
20N
40N
60N

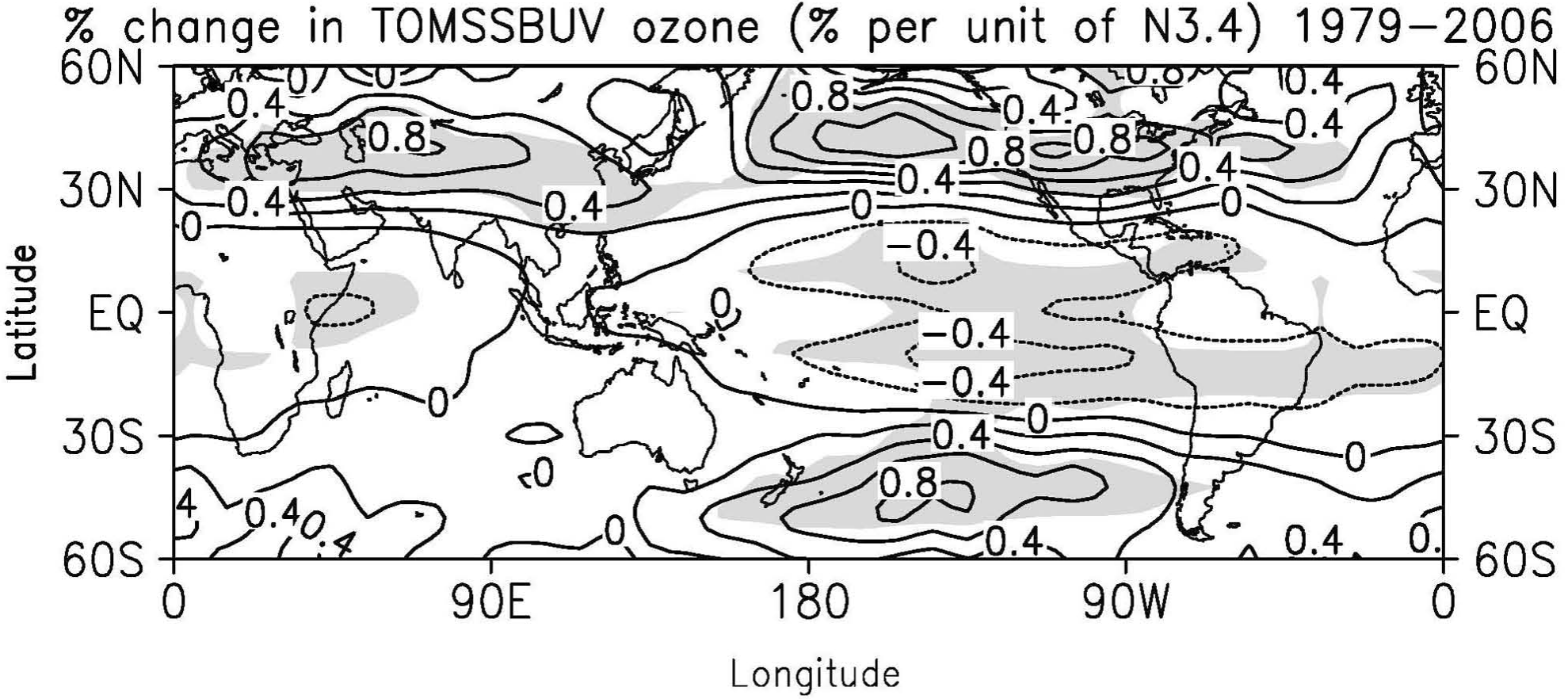
% change in TOMSSBUV ozone (% per unit of N3.4) 1979–2006
60N
30N
EQ
30S
60S
Latitude
0
90E
180
90W
0
Longitude

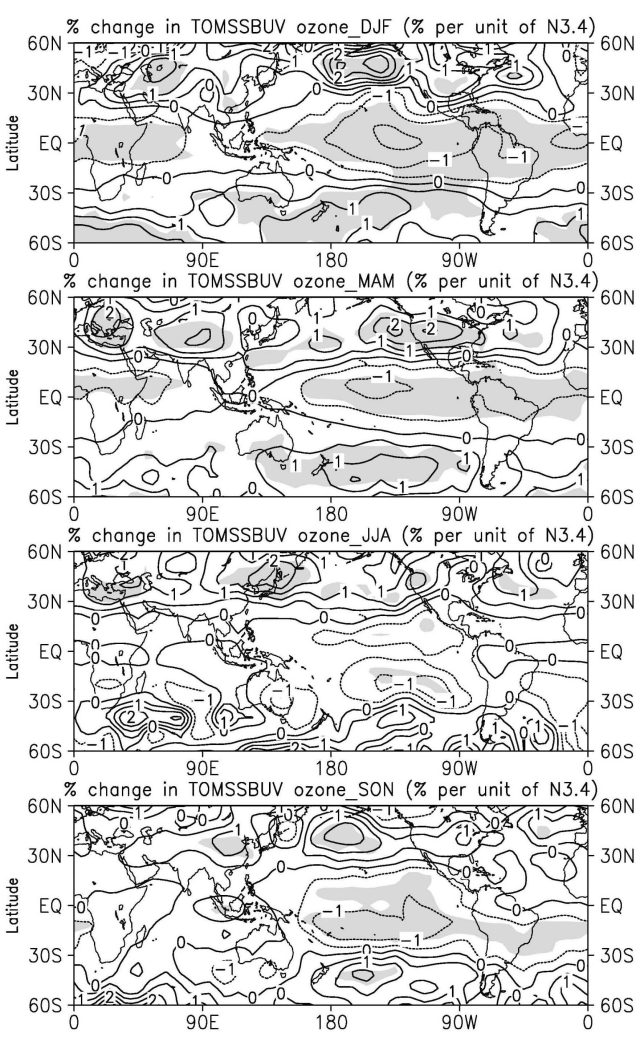
% change in TOMSSBUV ozone_DJF (% per unit of N3.4)
% change in TOMSSBUV ozone_MAM (% per unit of N3.4)
% change in TOMSSBUV ozone_JJA (% per unit of N3.4)
% change in TOMSSBUV ozone_SON (% per unit of N3.4)
Latitude
60N
30N
EQ
30S
60S
0
90E
180
90W

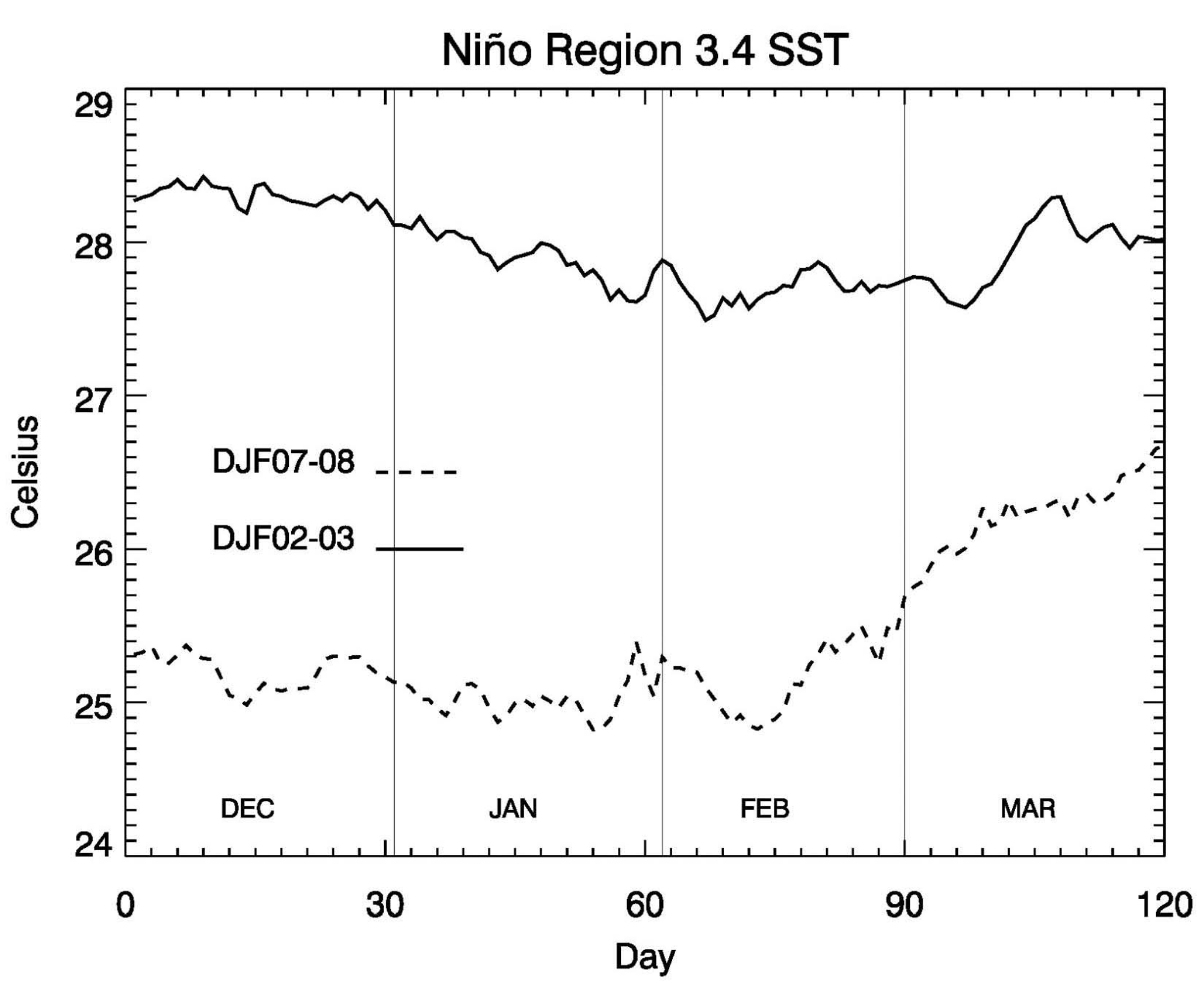
Niño Region 3.4 SST
29
28
27
26
25
24
Celsius
DJF07-08
DJF02-03
DEC
JAN
FEB
MAR
0
30
60
90
120
Day

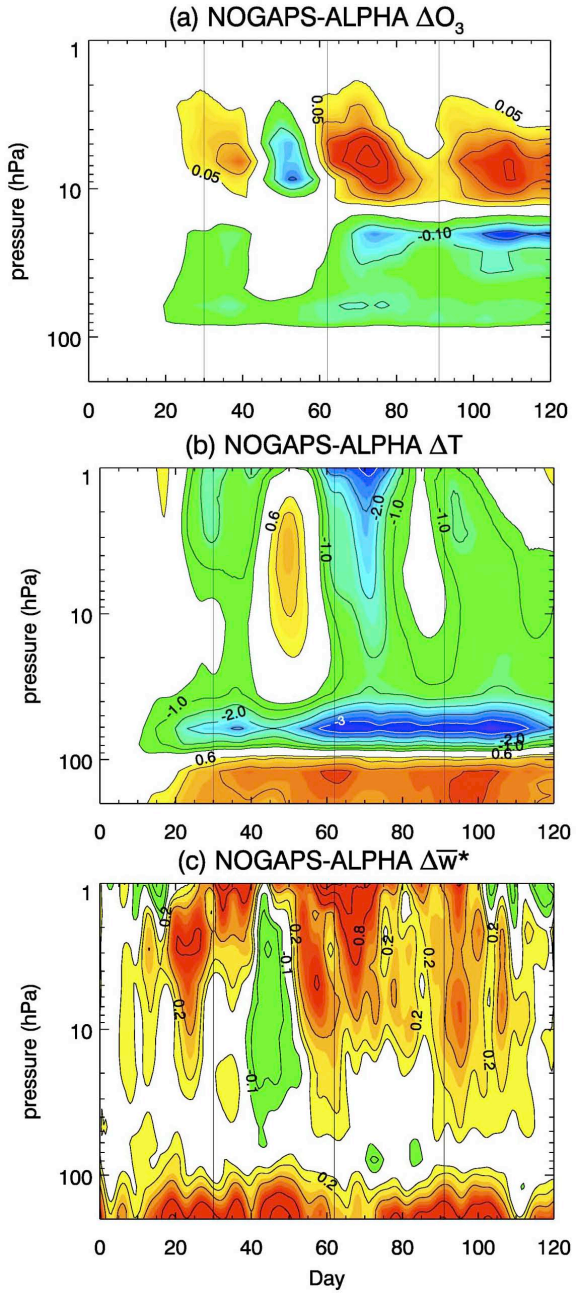
(a) NOGAPS-ALPHA ΔO3
pressure (hPa)
1
10
100
0
20
40
60
80
100
120
0.05
0.05
0.05
-0.10
(b) NOGAPS-ALPHA ΔT
pressure (hPa)
0.6
-1.0
-2.0
-1.0
-1.0
-1.0
-2.0
-3
-2.0
0.6
0.6
(c) NOGAPS-ALPHA Δw*
pressure (hPa)
0.2
0.1
0.8
0.2
0.2
0.2
0.2
0.2
0.2
0.2
0.1
0.2
Day

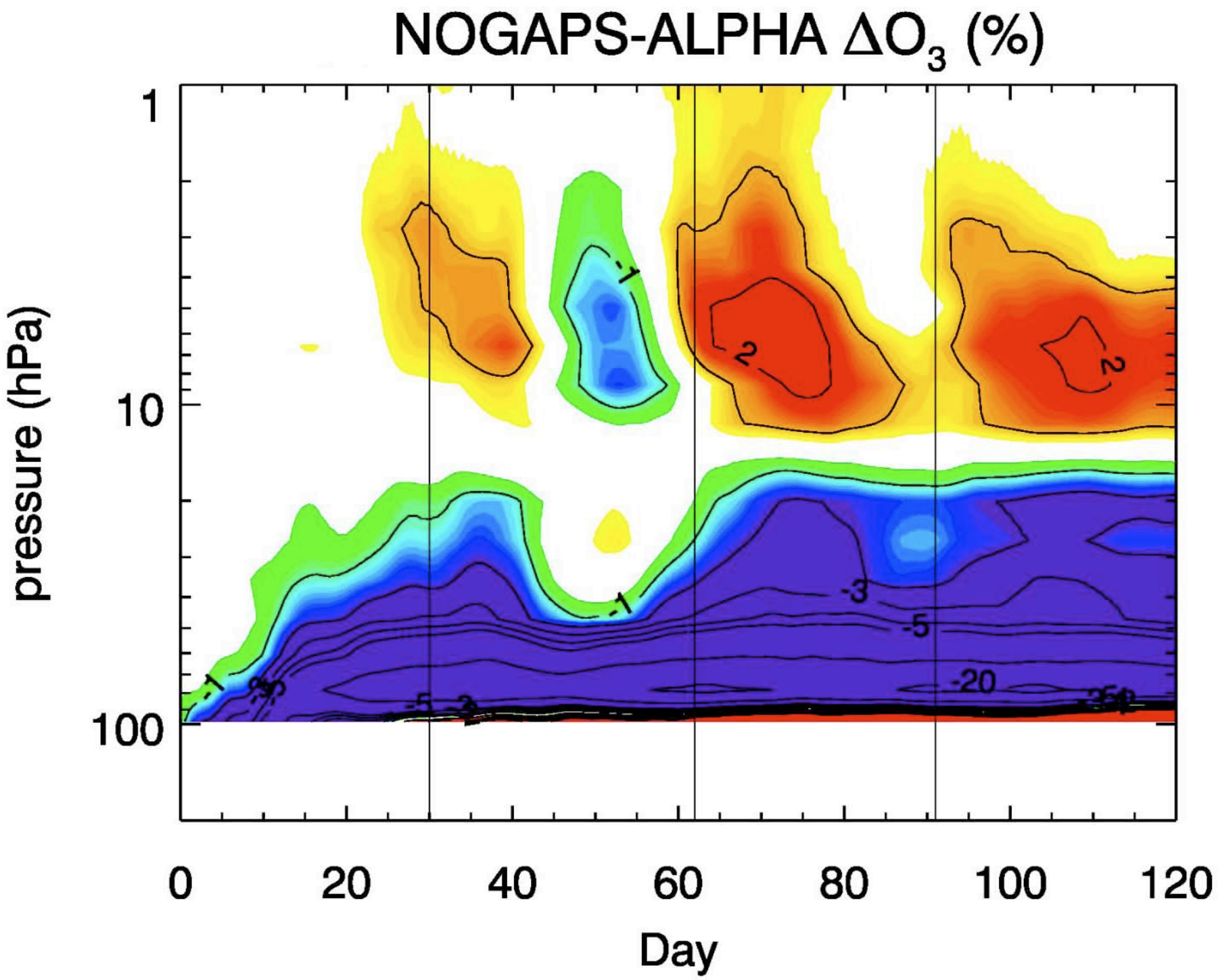
NOGAPS-ALPHA ΔO3 (%)
pressure (hPa)
1
10
100
0
20
40
60
80
100
120
Day
-1
2
-1
2
-3
-5
-20
-1
-5
-3

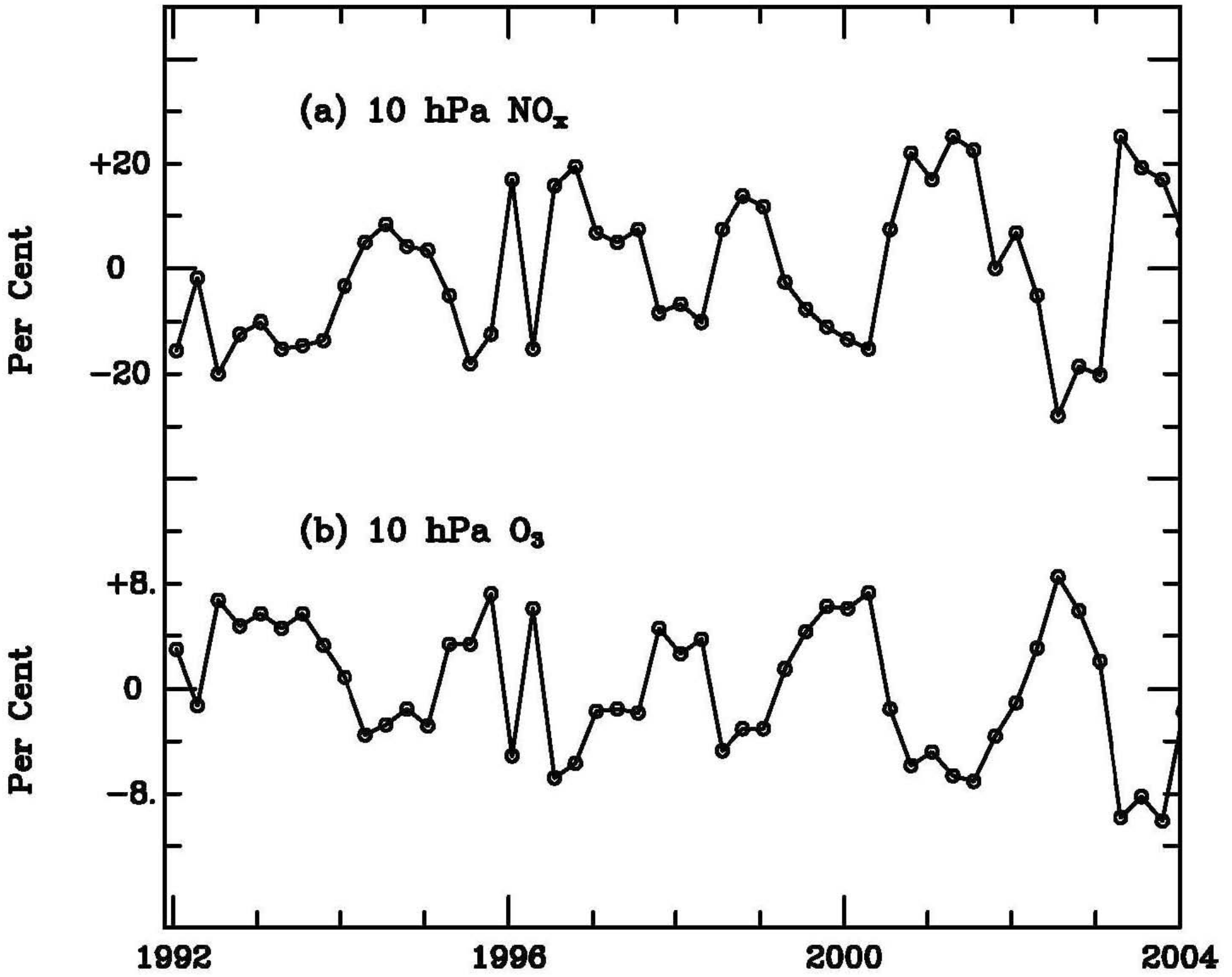
HALOE 3–Month Deviations, 5°S–5°N
(a) 10 hPa NOx
+20
0
–20
Per Cent
(b) 10 hPa O3
+8.
0
–8.
Per Cent
1992
1996
2000
2004